Article

Cell Reports

COA6 Is Structurally Tuned to Function as a Thiol-Disulfide Oxidoreductase in Copper Delivery to Mitochondrial Cytochrome *c* Oxidase

Graphical Abstract

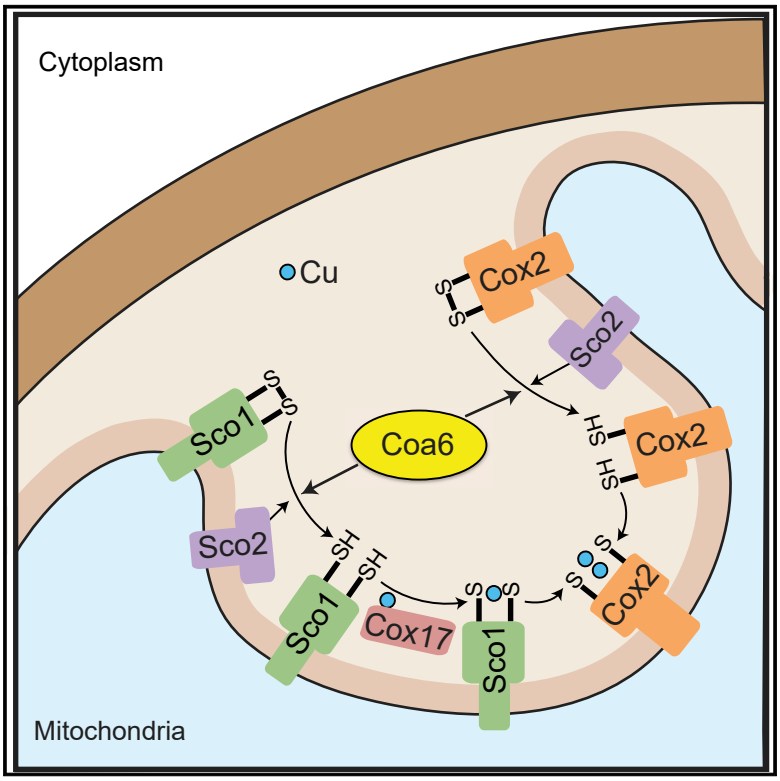

Authors

Shivatheja Soma, Marcos N. Morgada, Mandar T. Naik, ..., Scot C. Leary, Alejandro J. Vila, Vishal M. Gohil

Correspondence

vgohil@tamu.edu

In Brief

Soma et al. reports the solution structure of cytochrome *c* oxidase assembly factor COA6 and establishes that it functions as a thiol-disulfide oxidoreductase in a relay system that delivers copper to COX2, a copper-containing subunit of the mitochondrial cytochrome *c* oxidase.

Highlights

- COA6 is a coiled-coil-helix-coiled-coil-helix domain containing protein
- COA6 preferentially interacts with SCO1 over SCO2
- COA6 acts as a disulfide reductase of SCO1 and COX2
- COA6 function can be bypassed under hypoxic conditions

Soma et al., 2019, Cell Reports *29*, 4114–4126
December 17, 2019
https://doi.org/10.1016/j.celrep.2019.11.054

CellPress

OPEN ACCESS
CellPress

Cell Reports
Article

COA6 Is Structurally Tuned to Function as a Thiol-Disulfide Oxidoreductase in Copper Delivery to Mitochondrial Cytochrome *c* Oxidase

Shivatheja Soma,[1] Marcos N. Morgada,[2,8] Mandar T. Naik,[1,6,8] Aren Boulet,[3] Anna A. Roesler,[3] Nathaniel Dziuba,[1] Alok Ghosh,[1,7] Qinhong Yu,[4] Paul A. Lindahl,[1,5] James B. Ames,[4] Scot C. Leary,[3] Alejandro J. Vila,[2,9] and Vishal M. Gohil[1,9,10,*]

[1]Department of Biochemistry and Biophysics, MS 3474, Texas A&M University, College Station, TX 77843, USA
[2]Instituto de Biología Molecular y Celular de Rosario (IBR-CONICET), Área Biofísica, Departamento de Química Biológica, Facultad de Ciencias Bioquímicas y Farmacéuticas, Universidad Nacional de Rosario, Rosario (2000), Argentina
[3]Department of Biochemistry, Microbiology and Immunology, University of Saskatchewan, Saskatoon, SK S7N 5E5, Canada
[4]Department of Chemistry, University of California, Davis, Davis, CA 95616, USA
[5]Department of Chemistry, Texas A&M University, College Station, TX 77843, USA
[6]Present address: Department of Molecular Pharmacology, Physiology, and Biotechnology, Brown University, Providence, RI 02903, USA
[7]Present address: Department of Biochemistry, University of Calcutta, Kolkata 700019, India
[8]These authors contributed equally
[9]Senior author
[10]Lead Contact
*Correspondence: vgohil@tamu.edu
https://doi.org/10.1016/j.celrep.2019.11.054

SUMMARY

In eukaryotes, cellular respiration is driven by mitochondrial cytochrome *c* oxidase (CcO), an enzyme complex that requires copper cofactors for its catalytic activity. Insertion of copper into its catalytically active subunits, including COX2, is a complex process that requires metallochaperones and redox proteins including SCO1, SCO2, and COA6, a recently discovered protein whose molecular function is unknown. To uncover the molecular mechanism by which COA6 and SCO proteins mediate copper delivery to COX2, we have solved the solution structure of COA6, which reveals a coiled-coil-helix-coiled-coil-helix domain typical of redox-active proteins found in the mitochondrial inter-membrane space. Accordingly, we demonstrate that COA6 can reduce the copper-coordinating disulfides of its client proteins, SCO1 and COX2, allowing for copper binding. Finally, our determination of the interaction surfaces and reduction potentials of COA6 and its client proteins provides a mechanism of how metallochaperone and disulfide reductase activities are coordinated to deliver copper to CcO.

INTRODUCTION

Copper (Cu) is a redox-active transition metal that plays essential roles in cellular physiology by acting as a catalytic cofactor in numerous enzymatic reactions (Kim et al., 2008). One of the most critical Cu-containing enzymes is cytochrome *c* oxidase (CcO), a multimeric heme-Cu oxidase that is integral to the inner mitochondrial membrane and is the main site of cellular respiration (Ferguson-Miller and Babcock, 1996). CcO activity and its assembly depend on the formation of two Cu centers—Cu_A and Cu_B—on the COX2 and COX1 subunits, respectively (Tsukihara et al., 1995). These centers provide a molecular conduit for the transfer of electrons from reduced cytochrome *c* to molecular oxygen, the terminal step in mitochondrial respiration.

The high chemical reactivity and thiophilic nature of Cu ions present a challenge for its transport and insertion into target enzymes. Aqueous Cu ions can drive the production of deleterious hydroxyl radicals (Halliwell and Gutteridge, 1984) and can displace other metal ions from proteins, impairing their proper function and preventing its own delivery to cuproproteins (Foster et al., 2014; Macomber and Imlay, 2009). Moreover, the reduced oxidation state of cysteine ligands in cuproproteins, which coordinate Cu via their sulfhydryl groups, is necessary for Cu binding (Abriata et al., 2008). Not surprisingly, metallation of CcO is a complex process that requires several evolutionarily conserved proteins with distinct roles in Cu delivery and insertion (Soto et al., 2012; Timón-Gómez et al., 2018). For example, delivery of Cu to the cysteine-bridged binuclear Cu_A site requires at least four proteins– COX17, SCO1, SCO2, and COA6; all of which are either localized to the mitochondrial inter-membrane space (IMS) or anchored to the inner mitochondrial membrane with their functional domains facing the IMS (Vögtle et al., 2017). These proteins are part of a relay system, where Cu ions are sequentially transferred from COX17 to SCO1 and then to the Cu_A site of the COX2 subunit (Horng et al., 2004; Banci et al., 2008; Morgada et al., 2015). Structural and functional analyses of the yeast and human COX17 and SCO1 proteins have shown that they both coordinate Cu through their cysteinyl residues (Abajian et al., 2004; Abajian and Rosenzweig 2006; Banci et al., 2006, 2008) and act as metallochaperones (Banci et al., 2008; Horng et al., 2004; Morgada et al., 2015). Human SCO2 acts as a thiol-disulfide oxidoreductase of SCO1 *in vivo* and COX2 *in vitro* (Leary et al., 2009; Morgada et al., 2015). These

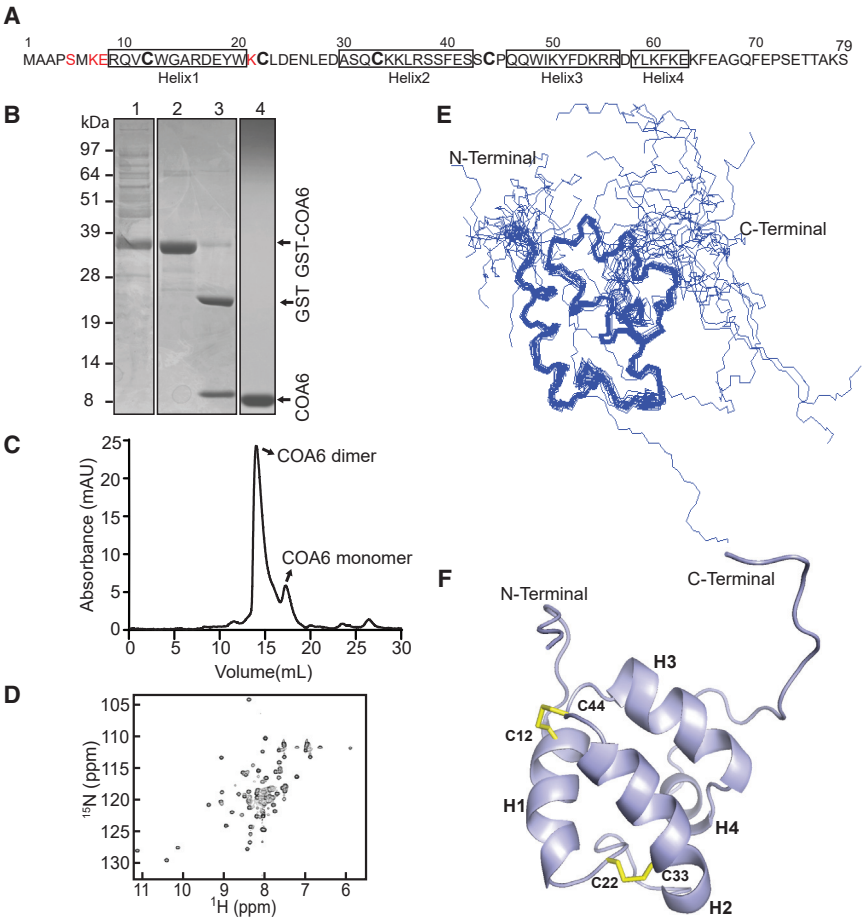

Figure 1. Solution Structure of Human COA6

(A) Primary structure of human COA6. No NMR assignments were achieved for the residues colored in red.

(B) SDS-PAGE analysis of the samples obtained during COA6 purification steps: lane 1, supernatant of lysate from *E. coli* expressing the COA6-GST fusion protein; lane 2, eluate containing COA6-GST from the GST binding column; lane 3, COA6-GST after cleaving the GST tag with thrombin; and lane 4, purified COA6 sample from gel filtration chromatography.

(C) Elution profile of purified COA6 from the Superdex 75 gel-filtration column.

(D) ^{1}H-^{15}N HSQC spectrum of human COA6.

(E) Ensemble of the 20 NMR solution structures of COA6 by backbone representation.

(F) Ribbon representation of human COA6 based on the lowest energy conformer of solution structures. Human COA6 has four helixes labeled as H1, H2, H3, and H4, and the two disulfide bonds between H1 and H2 are shown in yellow.

findings show that in addition to the metallochaperone activity of COX17 and SCO1, a thiol-disulfide oxidoreductase activity is essential for inserting Cu into the Cu_A site.

Recently, we reported that the poorly characterized CcO assembly factor COA6 is a novel member of the Cu delivery pathway to CcO (Ghosh et al., 2014). Subsequent biochemical and genetic interaction studies showed that COA6 interacts with SCO1, SCO2, and COX2, and that it has an overlapping function with SCO2 in the biogenesis of the Cu_A site (Ghosh et al., 2016; Pacheu-Grau et al., 2015; Stroud et al., 2015). Loss of COA6 in many organisms results in a severe CcO deficiency, demonstrating its conserved role in this pathway (Ghosh et al., 2014). Loss-of-function mutations in *COA6* in human mitochondrial disease patients result in fatal infantile cardiomyopathies, further highlighting its critical requirement in cellular respiration (Baertling et al., 2015; Calvo et al., 2012). Pathogenic mutations have also been reported in the COA6-interacting partners SCO1 and SCO2, and *SCO* patients present with similar, early onset clinical syndromes owing to an isolated CcO deficiency (Papadopoulou et al., 1999; Stiburek et al., 2009). Although these observations emphasize the centrality of this pathway to CcO biogenesis, the precise biochemical function of COA6 and the nature of its interactions with various partners during Cu_A site maturation are still largely unknown.

Here, we address these unknowns by a combination of a nuclear magnetic resonance (NMR)-based structural determination and *in vitro* and *in vivo* mechanistic biochemistry. We show that COA6 adopts a coiled-coil-helix-coiled-coil-helix (CHCH) domain, preferentially interacts with SCO1, and exhibits thiol-disulfide oxidoreductase activity both *in vitro* and *in vivo*, with SCO1 and COX2 being its client proteins. We further demonstrate that COA6 is not a Cu-binding protein under physiological conditions and that its enzymatic activity is independent of metalation state. Collectively, our data suggest a mechanistic picture in which COA6 and SCO2 act as disulfide reductases during the stepwise transfer of Cu from Cox17 to the Cu_A site.

RESULTS

Human COA6 Is a Helical Protein with a CHCH Domain

To uncover the molecular function of COA6, we first solved the solution structure of human COA6 isoform 3, hereafter referred to as COA6 (Figure 1A). We chose isoform 3 for our structural studies because it encompasses the most well-conserved region of the full-length protein and it contains the primary structure that functionally complements yeast *coa6Δ* cells (Ghosh et al., 2016). Human COA6 was expressed as a glutathione S-transferase (GST) fusion protein and the GST tag was cleaved with thrombin protease to release free COA6 (Figure 1B). Subsequent gel-filtration analysis suggests that COA6 exists predominantly as an ~18-kDa dimer (Figure 1C). Isotope-enriched COA6 samples were then prepared and the structure determined using distance and angle restraints obtained from 2D and 3D heteronuclear NMR spectra. The ^{1}H-^{15}N heteronuclear signal quantum correlation (HSQC) spectrum of COA6 shows well-dispersed

resonances, indicative of a folded protein as well as parts lacking stable structure (Figure 1D; PDB: 6NL3). The unstructured nature of N- and C-terminal residues is evident from ^{1}H-^{15}N NOE data (Figures S1A–S1C). Sixty-seven out of the expected 75 ^{15}N backbone amide resonances were detected and approximately 90% of all detectable carbon, nitrogen, and hydrogen nuclei were assigned.

To determine if dimerization of COA6 is affected by its concentration, we acquired the ^{1}H-^{15}N HSQC spectrum of COA6 at varying protein concentrations (Figure S1D). Analysis of the relative chemical shift perturbations at the lowest compared to the highest COA6 concentration (Figure S1E) indicates that the residues in helix 3 of COA6 are likely involved in dimerization. Comparable gel-filtration elution profiles in the presence and absence of tris(2-carboxyethyl)phosphine (TCEP) argue that the dimerization of COA6 is unaffected by a strong reducing agent (Figure S1F). This finding suggests that dimerization is not due to inter-disulfide bonding between cysteine residues of each COA6 monomer.

We obtained an ensemble of 20 COA6 structures in excellent agreement with experimental restraints (Table S1). This ensemble indicates that the N and C termini of COA6 (residues 1-8 and 65-79, respectively) are unstructured (Figure 1E). The lowest energy conformer of COA6 shows that the compact core, encompassing residues 9-64, is entirely helical and is composed of four helices, with the first two, H1 and H2, stabilized by a pair of disulfide bonds (Figure 1F). The CB chemical shifts of each cysteine (C12, 37.566 ppm; C22, 32.450 ppm; C33, 32.006 ppm; and C44, 45.634 ppm) were interpreted alongside NOESY patterns to deduce disulfide pairing (Sharma and Rajarathnam, 2000). Addition of TCEP to purified COA6 produced only localized changes in the HSQC spectrum, including splitting of the W20 side chain peak (Figures S1G and S1H). Since W20 is proximal to the C22-C33 disulfide, this phenomenon is likely due to the reduction of this disulfide bond. COA6 exhibits a CHCH domain reminiscent of many mitochondrial IMS proteins with proposed roles in redox chemistry (Banci et al., 2009b). To further determine if the structural features of COA6 are conserved in yeast Coa6, we analyzed the ^{1}H-^{15}N HSQC spectrum and chemical shift index (CSI) of recombinant yeast Coa6 and found that it is also a helical protein (Figures S2A and S2B).

Mapping *COA6* Patient Mutations onto the COA6 Structure Uncovers the Structural Basis of Pathogenicity

Mutations in *COA6* have been reported in two unrelated human mitochondrial disease patients: one with compound heterozygous mutations (W59C and E87X) (Calvo et al., 2012) and the other with a homozygous missense mutation (W66R) (Baertling et al., 2015). These residues are highly conserved, suggesting their essential function (Figure 2A). To understand how these mutations affect COA6 function, we mapped the mutated residues onto the COA6 structure. The truncation mutation (E87X) clearly disrupts the CHCH domain by removing a large portion of the protein from helix 2 onward (Figures 2A and 2B). The other two mutations, W59C and W66R, are found within the first helix of COA6, where the side chains of each tryptophan face the bulk solvent, suggesting that these residues may facilitate interactions with their client proteins (Figure 2B).

To further test the effect of these two missense mutations on COA6 function, we introduced patient mutations into a human-yeast chimera (hyCOA6) that consists of the bulk of the human protein and the N-terminal 24 amino acid residues of yeast Coa6 to facilitate mitochondrial targeting (Figure 2A). As expected based on our previous study, the respiratory growth of *coa6Δ* cells was restored by hyCOA6 (Ghosh et al., 2016) but not by either of the tryptophan variants, suggesting that these missense mutations disrupt COA6 function or expression (Figure 2C). To distinguish between these two possibilities, we measured the expression of COA6 mutants and found that while $hyCOA6_{W33R}$ and the truncated protein $hyCOA6_{E54X}$ are undetectable, $hyCOA6_{W26C}$ is expressed and localizes to mitochondria (Figures 2D and 2E). These data suggest that the W26C mutation perturbs COA6 function. To further study the effect of these mutations within the context of human cells, we overexpressed the wild-type (WT) and mutant alleles of *COA6* in control and *COA6* patient fibroblasts and found that the W66R variant fails to rescue CcO activity (Figure 2F). In contrast, expression of the W59C mutant leads to a partial recovery of CcO activity and COX2 levels (Figures 2D and 2E), consistent with a previous report (Stroud et al., 2015). Curiously, COA6 abundance in patient cells overexpressing the W59C and W66R mutants was comparable and at the lower limits of detection (Figure 2G). It seems that in most cell types residual levels of the partially functional W59C allele are not sufficient to support CcO assembly and mitochondrial respiration because *coa6Δ* cells expressing the W59C variant do not exhibit respiratory growth (Figure 2C) and the human patient with the W59C mutation exhibits a severe CcO deficiency in cardiac tissue (Calvo et al., 2012). Taken together, these data strongly suggest that the conserved tryptophans are critical for COA6 stability and possibly for their interactions with client proteins.

COA6 Preferentially Interacts with SCO1 over SCO2

Previous studies from yeast and human cell lines have shown that COA6 interacts with COX2 and SCO proteins *in vivo* (Ghosh et al., 2016; Pacheu-Grau et al., 2015; Stroud et al., 2015). Genetic and physical interaction studies demonstrate that yeast Coa6 interacts with both Sco1 and Sco2 (Ghosh et al., 2016). However, studies of human COA6 are less conclusive, with one group reporting that COA6 physically interacts only with SCO2 (Pacheu-Grau et al., 2015) and another group reporting interactions only with SCO1 (Stroud et al., 2015).

Given the uncertainty surrounding the relative affinity of COA6 for its interacting partner(s), we decided to further investigate COA6 interactions with the SCO proteins by conducting competitive binding analysis using size-exclusion chromatography (SEC). First, we determined the elution profiles of each protein in isolation. The elution profile for COA6 shows a right-tailing-effect (Figure 3A), suggesting equilibrium between monomeric and dimeric forms (~18 kDa) of the protein. The soluble domains of SCO1 and SCO2 behave as monomeric 20- and 17.6-kDa proteins, respectively (Figures 3B and 3C).

We then obtained elution profiles for different mixtures of these proteins. An equimolar mixture of COA6 and SCO1 led

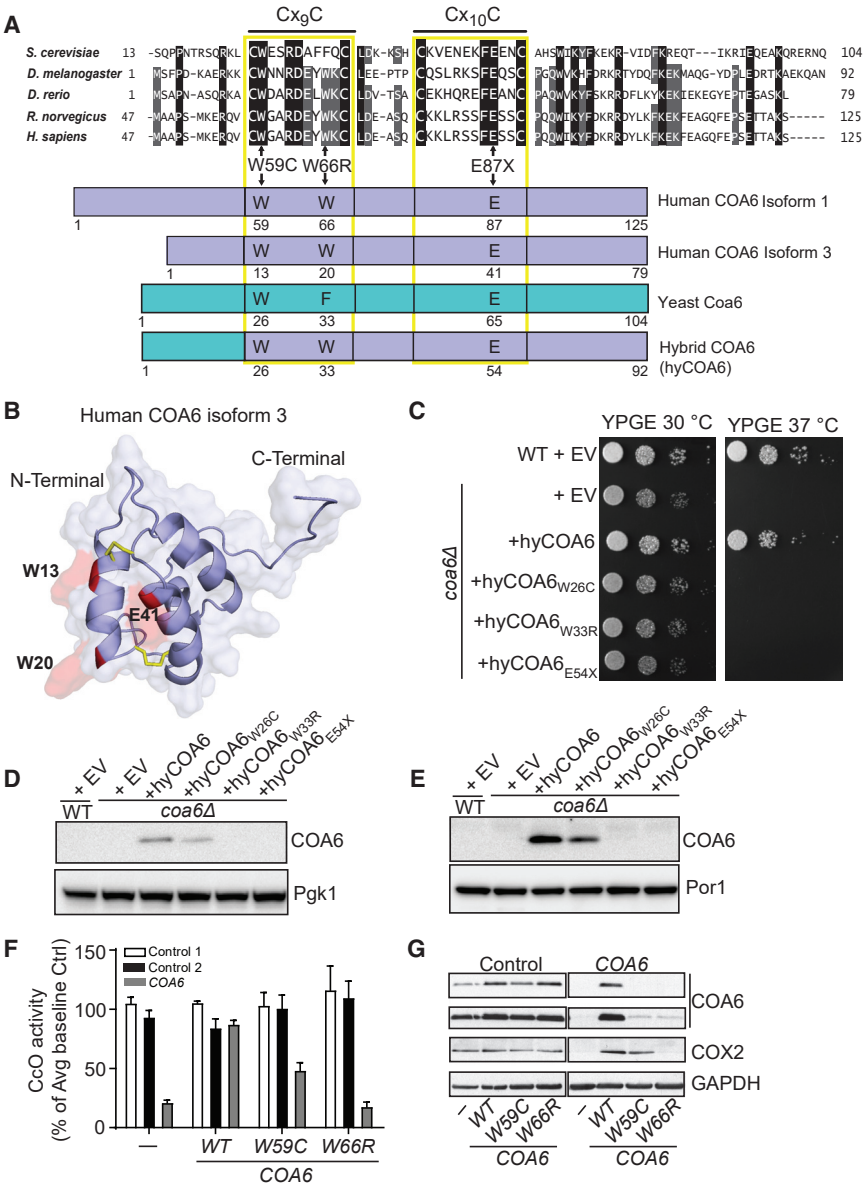

Figure 2. Mapping *COA6* Patient Mutations onto the COA6 Structure

(A) Sequence alignment of the conserved region of COA6 across indicated model organisms. Horizontal lines above Cx_9C and $Cx_{10}C$ residues show the conserved $Cx_9Cx_nCx_{10}C$ motif. Schematic representation of the yeast-human hybrid COA6 (hyCOA6) protein, where the sequences from yeast Coa6 and human COA6 are shown in cyan and blue, respectively. Arrows indicate amino acid residues that were mutated in human *COA6* patients and the corresponding residues in the hyCOA6 protein.

(B) Ribbon representation of *COA6* patient mutations mapped onto the COA6 structure in red.

(C) Wild-type (WT) and *coa6Δ* cells transformed with empty vector (EV) or vector-expressing hyCOA6 or hyCOA6 harboring patient mutations (W26C, W33R, and E54X) were serially diluted and seeded on YP glycerol-ethanol (YPGE) plates. Cells were grown at 30°C and 37°C for 5 days.

(D and E) SDS-PAGE/western blot analysis of whole cell (D) and mitochondrial protein (E) extracts from *coa6Δ* cells expressing wild-type or mutant hyCOA6 proteins. Por1 and Pgk1 were used as loading controls.

(F) Human control and *COA6* patient cell lines were transduced with cDNAs expressing either WT or pathogenic variants of COA6 followed by measurement of CcO activity. Data are represented as mean ± SEM, n = 3.

(G) SDS-PAGE/western blot depicting COA6, COX2, and GAPDH (loading control) levels in protein lysate from control and *COA6* cell lines as indicated in (D). The data shown are representative of at least three independent replicates.

to the formation of a complex of ~27 kDa, and the absence of a peak corresponding to COA6 alone, indicating that all of the COA6 is found within the higher molecular weight complex (Figure 3D). Excess SCO1 appears as a shoulder on the chromatogram (Figure 3D). Based on the apparent molecular weight of the complex, COA6 appears to interact with SCO1 as a monomer and with relatively high affinity. Next, we analyzed an equimolar mixture of COA6 and SCO2 and observed the formation of higher molecular weight complexes, suggesting that SCO2 can also interact with COA6 (Figure 3E).

To better probe the competitive binding of SCO1 and SCO2 with COA6, a mixture of all three proteins was prepared and analyzed by SEC. Three distinct peaks were identified in the elution profile (Figure 3F). Through curve fitting, we compared this elution profile with traces of each individual protein (Figure 3G) and with traces of the mixtures of two proteins (Figure 3H), and found that the high molecular weight peak corresponds to the SCO1:COA6 complex and the remaining two peaks correspond to SCO1 and SCO2 alone. To confirm the constituents of the elution profile, we performed an immunoblot analysis of each eluted fraction to detect both SCO proteins and COA6. We found that the majority of COA6 co-elutes with SCO1 (Figure 3I), strongly suggesting that at least *in vitro* SCO1 is the dominant interacting partner of COA6.

COA6 Uses a Largely Non-polar Interface to Interact with SCO1

To identify the surfaces that facilitate interactions between COA6 and SCO1, we compared HSQC spectra of ^{15}N-labeled COA6 obtained in the presence and absence of unlabeled SCO1. A comparison of the two spectra identified pronounced chemical shift perturbations in residues 49-55 present in helix 3 and residues 65-69 that form a β-hairpin turn of COA6 (Figures 4A and 4B). Most of these COA6 residues are non-polar, suggesting

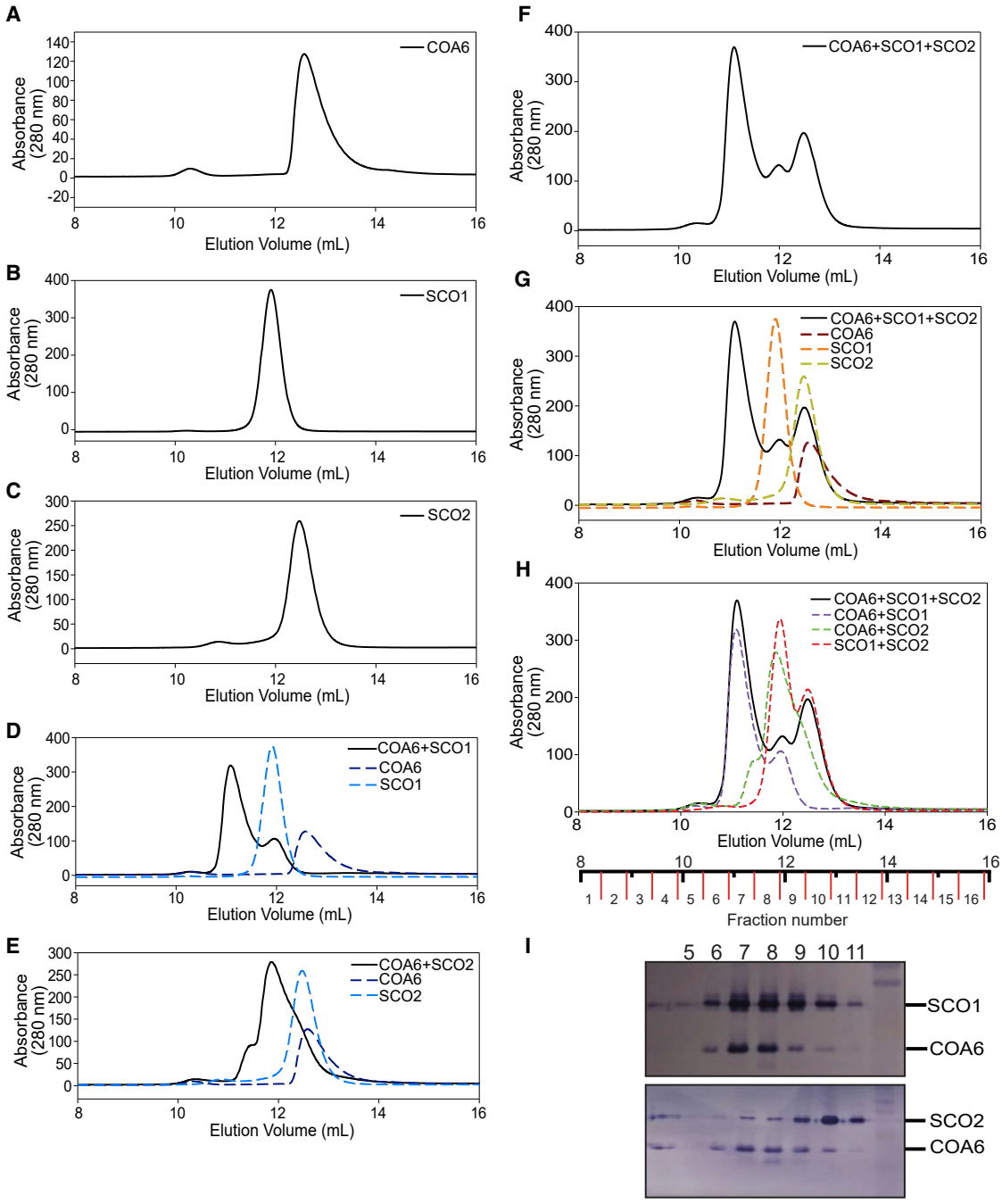

Figure 3. Human COA6 Exhibits a Stronger Interaction with SCO1 than SCO2

(A–C) Size exclusion chromatography elution profiles of (A) COA6, (B) SCO1, and (C) SCO2.

(D–H) Elution profiles of the indicated mixtures of proteins (solid lines), compared to simulations of the indicated individual proteins or mixtures of two or more proteins (dotted lines).

(I) SDS-PAGE/western blot analysis of different fractions from size exclusion chromatogram shown as the solid black line in (F)–(H).

hydrophobic interactions between COA6 and SCO1. Notably, we did not detect perturbations in the N-terminal residues of COA6, around the patient mutations corresponding to W20, suggesting that these residues are not critical for the interaction with SCO1 (Figures 4A and 4B).

To obtain complementary information about the interaction surface on SCO1, we performed the reciprocal experiment where HSQC spectra of ^{15}N-labeled SCO1 were obtained in the presence and absence of unlabeled COA6. This led to the identification of a number of non-polar residues present on the

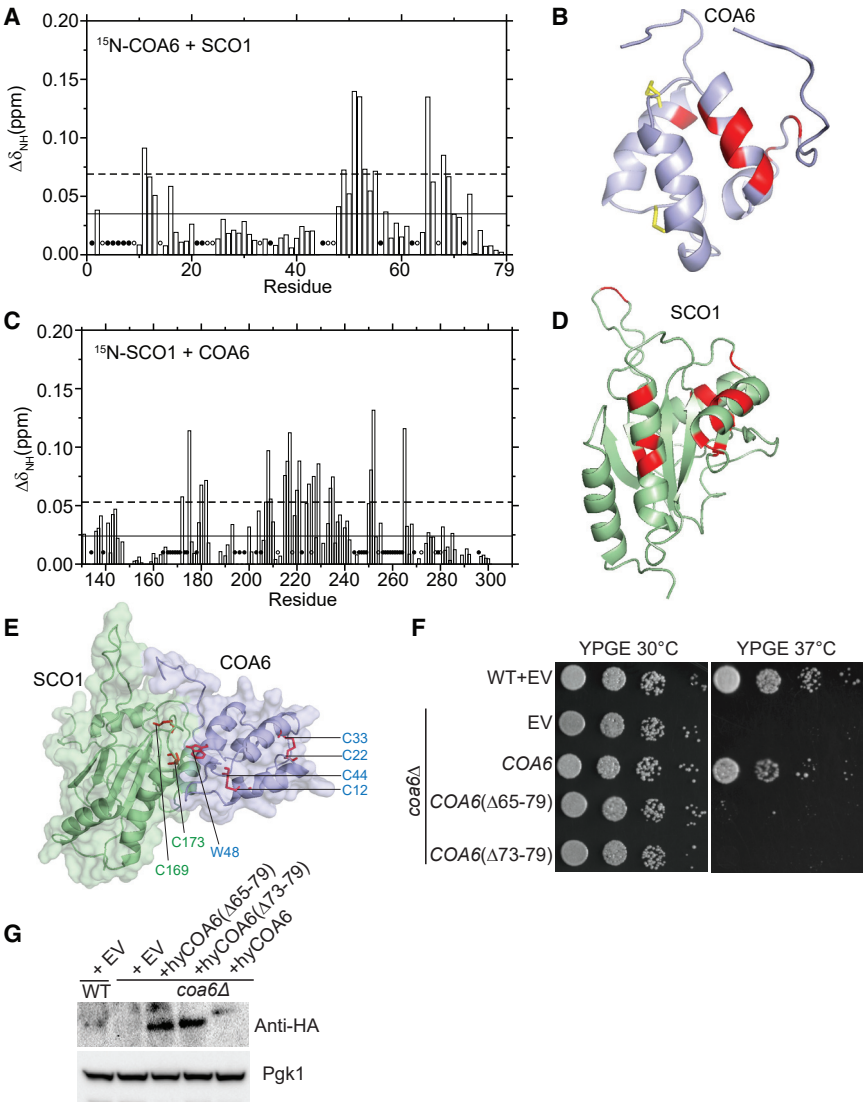

Figure 4. Mapping the Surfaces That Mediate Interactions between COA6 and SCO1

(A) Average chemical shift perturbation of ^{15}N-labeled COA6 upon addition of equimolar unlabeled SCO1. Horizontal solid line, mean chemical shift perturbation; dashed line, mean + SD of chemical shift perturbation for all residues; solid circles, unassigned residues; and open circles, residues with broadened peaks upon complex formation.

(B) COA6 residues with significant chemical shift perturbations are colored in red on a ribbon representation of COA6.

(C) Chemical shift perturbation of ^{15}N-labeled SCO1 residues upon addition of equimolar unlabeled COA6, as displayed in (A).

(D) SCO1 residues with significant chemical shift perturbations are colored in red on a ribbon representation of SCO1.

(E) A HADDOCK docking model of the COA6:SCO1 complex generated using chemical shift perturbation (CSP) data. The side chain of the COA6 tryptophan (W48) and the indicated cysteine residues of COA6 and SCO1 are shown in stick representations in red.

(F) WT and *coa6Δ* cells transformed with empty vector (EV) or vector expressing either full-length or truncated hyCOA6. Transformants were serially diluted on agar plates and grown for 5 days.

(G) SDS-PAGE/western blot analysis of protein extracts from *coa6Δ* cells expressing wild-type or truncated mutants of hyCOA6. Pgk1 was used as loading control.

same face of the SCO1 surface (Figures 4C and 4D). Interestingly, the surface that SCO1 uses to interact with COA6 is also highly conserved in SCO2 (Figure S3A), suggesting that COA6 is capable of interacting with each SCO protein via a common surface (Figure S3). Using the chemical shift perturbation data, we generated a hypothetical docking model for the SCO1:COA6 complex using High Ambiguity Driven protein-protein Docking (HADDOCK) (de Vries et al., 2010). This model shows that the Cu-binding cysteines of SCO1 (Cys169 and Cys173) are located in a U-shaped turn region that makes direct intermolecular contact with the H3 helix of COA6 (Figure 4E). In particular, the indole side chain of W48 from COA6 (highlighted red in Figure 4E) is within 3 Å of the sulfhydryl side chain of Cys173 from SCO1 (Figure 4E). The indole side chain of W48 is also located halfway between Cys173 of SCO1 and Cys44 of COA6, suggesting that W48 may bridge or otherwise relay electrons from the Cys12/Cys44 disulfide bridge of COA6 to the Cu-binding cysteines of SCO1 (Cys169/Cys173). The COA6 and SCO1 intermolecular structural interaction is largely composed of hydrophobic residues localized to the H3 helix and the C-terminal tail of COA6 (Figure 4E). To test the validity of the interaction model, we generated two truncated forms of COA6 by deleting residues 64-79 (COA6Δ64-79) and residues 72-79 (COA6Δ72-79) from the C terminus. We confirmed that both the truncated forms of COA6 are expressed but are not functional, likely due to loss of their interaction with SCO1 (Figures 4F and 4G). Superimposition of the known missense mutations in SCO1 and SCO2 onto their ribbon diagrams further suggests that at least some of the pathogenic variants (e.g., SCO1 P174L, SCO2, and E140K) are close to the mapped interacting residues in COA6 (Figures S3B and S3C). Taken together, interaction mapping and genetic complementation data suggest that H3 and C-terminal residues of COA6 are critical for its interaction with SCO1.

COA6 Function Can Be Bypassed in a Reducing Environment

Although previous work has shown that human COA6 binds Cu with high affinity *in vitro* (Stroud et al., 2015), suggesting a possible metallochaperone function, Cu was not detected in the purified COA6 samples that we used for our structural

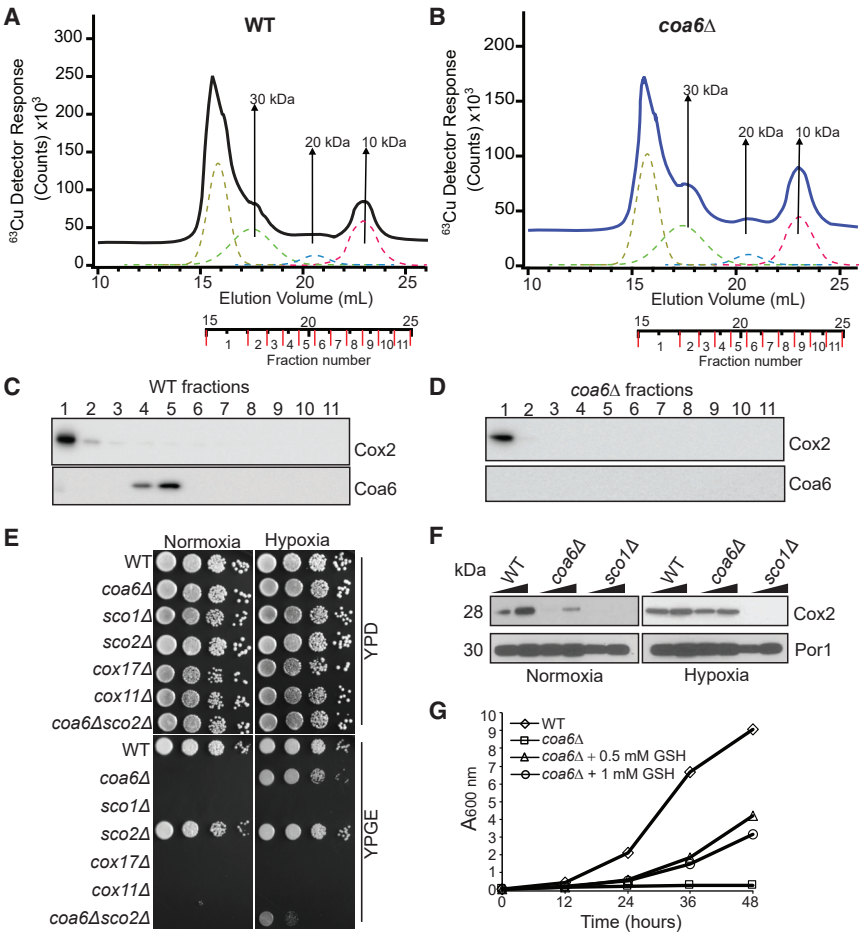

Figure 5. A Reducing Environment Rescues the Respiratory Growth of *coa6Δ* Cells

(A and B) Cu traces from online LC-ICP-MS of solubilized mitochondrial extracts from WT (A) or *coa6Δ* (B) cells. The dotted lines indicate simulated curves generated by peak fitting.

(C and D) SDS-PAGE/western blot depicting Cox2 and Coa6 protein levels in the different LC-ICP-MS fractions of WT (C) and *coa6Δ* (D) soluble mitochondrial extracts.

(E) Serially diluted WT, *coa6Δ*, *sco1Δ*, *sco2Δ*, *cox17Δ*, *cox11Δ*, and *coa6Δsco2Δ* cells were spotted on YP dextrose (YPD) and YP glycerol-ethanol (YPGE) plates and grown under normoxic or hypoxic (4% O_2) conditions.

(F) Western blot of Cox2 in the indicated yeast strains. Por1 was used as a loading control.

(G) WT and *coa6Δ* cells were cultured in YPGE medium at 37°C in the presence or absence of reduced glutathione (GSH) at the indicated concentrations. The cell density was measured spectrophotometrically at the indicated time points. These data are representative of at least three independent replicates.

studies. We therefore sought to definitively determine the Cu-binding properties of COA6. To do this, we first utilized a custom-built online liquid chromatography-inductively coupled plasma mass spectrometry (LC-ICP-MS) system, which allows simultaneous detection of Cu and protein in elution fractions obtained from SEC. When purified COA6 was applied to this LC-ICP-MS system, we detected a major peak at A_{280} corresponding to the COA6 dimer, although the peak was asymmetric and exhibited a right-tailing-effect, suggesting minor contributions from a monomeric species (Figure S4A). We did not detect any Cu peaks in the chromatogram, indicating that recombinant COA6 does not bind endogenous Cu from *E. coli* (Figure S4A). When purified COA6 was reconstituted with $CuSO_4$ and reduced glutathione as described previously (Stroud et al., 2015), we detected two major A_{280} peaks corresponding to a dimer and a low-intensity higher-molecular-weight species that likely corresponds to an aggregate of COA6 and Cu (Figure S4B). Indeed, the Cu peak was detected in the same fractions as COA6, with excess Cu found in the high-molecular-weight COA6 aggregates (Figure S4B). Thus, upon reconstitution in the presence of reduced glutathione, COA6 can bind Cu; however, we suspected that this was not the physiological form of the protein.

To address this issue, we tested whether Cu can bind Coa6 *in vivo* by analyzing yeast mitochondrial fractions. Lysates from anaerobically purified WT and *coa6Δ* mitochondria were subjected to LC-ICP-MS to identify Cu-specific peaks using a method we recently described (Nguyen et al., 2019). In WT mitochondria, we detected four Cu peaks, including one at the void volume and the others associated with masses of circa 30, 20, and 10 kDa (Figure 5A). *coa6Δ* samples exhibited nearly identical Cu peaks in the region associated with the same masses (Figure 5B). Notably, none of these Cu peaks corresponds to the fractions containing Coa6 (Figures 5C and 5D). The lack of any difference in the Cu peaks in the WT and *coa6Δ* mitochondrial lysates suggests that Coa6 does not bind Cu under physiological conditions in yeast cells and is therefore unlikely to act as a Cu metallochaperone.

The presence of a CHCH domain in the COA6 structure is consistent with a redox role for the protein in Cu_A site maturation, because the CHCH domain has been proposed to represent the minimal oxidoreductase domain, and a number of mitochondrial IMS proteins with this domain are indeed redox active (Banci et al., 2009a, 2009b). To begin investigating the potential redox role for COA6 in Cu delivery to CcO *in vivo*, we utilized hypoxic (4% O_2) conditions (Bihlmaier et al., 2007) to counter the oxidizing environment of the mitochondrial IMS (Hu et al., 2008). *coa6Δ* and other mutants involved in Cu delivery to CcO were cultured under normoxic or hypoxic conditions in both fermentable and respiratory media. The respiratory growth of *coa6Δ* was almost fully rescued in hypoxic yeast, while that of yeast strains lacking proteins with established Cu metallochaperone activity (*sco1Δ*, *cox17Δ*, and *cox11Δ*) was not (Figure 5E). This finding suggests that hypoxia cannot replace a metallochaperone function and is likely more specific to rescuing the

functional deficiency in redox-related proteins (Figure 5E). Consistent with this idea, we also observed a partial rescue of *coa6Δ* yeast that also lacks Sco2, a protein with an established disulfide reductase activity in Cu delivery to CcO (Figure 5E). We were unable to test the effect of hypoxia on a *sco2Δ* strain directly, because yeasts lacking Sco2 do not have a pronounced respiratory growth-related phenotype (Figure 5E).

The respiratory growth defect of *coa6Δ* cells has been attributed to a decrease in the levels of Cox2, which degrades rapidly when Cu delivery to CcO is impeded (Ghosh et al., 2014; Pacheu-Grau et al., 2015). Therefore, to test whether Cu delivery to Cox2 is restored under hypoxic conditions, we measured Cox2 abundance in *coa6Δ* cells and found that it was indeed restored to the WT levels (Figure 5F). Moreover, exogenous supplementation of a normoxic culture with reduced glutathione (GSH) also partially rescued respiratory growth of *coa6Δ* cells (Figure 5G), further supporting a redox role for Coa6 in the Cu delivery process. Taken together, these results strongly suggest that Coa6 has a redox as opposed to a metallochaperone function in Cu delivery to Cox2.

COA6 Acts as a Disulfide Reductase of SCO and COX2 Proteins

Previous work on the biogenesis of the prokaryotic Cu_A center of heme-Cu oxidases established the requirement for both Cu metallochaperones and disulfide reductases (Abriata et al., 2008). The presence of a CHCH domain, its redundancy in a hypoxic environment, and its overlapping function with SCO2 (Ghosh et al., 2016) all argue that COA6 harbors disulfide reductase activity. However, the redox potential of COA6 is unknown. To determine whether reduction of COX2 and SCO disulfides by COA6 is thermodynamically favorable, we measured the reduction potential of the ox/red COA6 couple using the DTT_{ox}:DTT_{red} redox couple as a calibrant, and found that at −330 mV (pH 7.0) it is lower than that of SCO1 (−280 mV) and COX2 (−290 mV) (Figures 6A and 6B). The reduction potential of SCO2 has previously been shown to be < −300 mV (Banci et al., 2007). These reduction potential values suggest that both COA6 and SCO2 can reduce SCO1 and COX2 in a thermodynamically favorable manner.

We then tested whether COA6 can effectively reduce the disulfide bonds of Cu-coordinating cysteines of its interacting partners. To do this, we used a thiol-alkylating reagent 4-acetamido-4′-maleimidylstilbene-2,2′-disulfonic acid (AMS), which selectively reacts with free thiols on proteins to form a protein-AMS adduct. This modification increases the protein mass by ~0.5 kDa per free thiol. The additional mass leads to an upward shift on an SDS-PAGE gel (Figure 6C). Utilizing this assay, we observed that a 1-h co-incubation of reduced COA6 with either of the oxidized SCO proteins led to the appearance of two SCO-specific bands in the AMS-treated samples (Figure 6D). This observation suggests that COA6 can reduce the disulfides of SCO proteins, generating free sulfhydryl groups that then react with AMS. Similarly, we found that COA6 can also reduce the cysteines of COX2 (Figure 6E).

Finally, to corroborate these *in vitro* findings, we tested the redox state of the cysteinyl thiols of SCO proteins *in vivo* in *COA6* patient fibroblasts using AMS and a second alkylating agent iodoacetamide (IAM). As shown previously, the cysteinyl sulfurs of SCO1 and SCO2 proteins exist as a mixed redox population in control fibroblasts that is composed of both oxidized and reduced thiols (Figure 6F) (Leary et al., 2009). Strikingly, mutations in *COA6* significantly skew the relative ratio of reduced to oxidized cysteinyl sulfurs of SCO1, with the oxidized species predominating (Figure 6F). In contrast, the ratio of oxidized-to-reduced sulfur species of SCO2 was comparable in control and *COA6* patient fibroblasts (Figure 6F). Taken together, these findings provide further evidence that COA6 acts as a disulfide reductase *in vivo* and suggest that SCO1 is one of its substrates.

To determine how the redox function of COA6 affects the synthesis and stability of COX2, we performed pulse-chase labeling of mitochondrial DNA-encoded proteins in control, *COA6*, *SCO1*, and *SCO2* patient fibroblasts. Consistent with our previous studies, we found that COX2 is synthesized normally in *SCO1-1* cells but is rapidly turned over during the chase (Cobine et al., 2006), while its synthesis is attenuated in *SCO2* cells yet it accumulates during the chase (Leary et al., 2009) (Figure S5). The profile of COX2 synthesis and degradation in *COA6* patient fibroblasts most closely mirrors that observed for *SCO2* cells (Figure S5), a result that would be expected if COA6 has a similar biochemical function to that of SCO2, which has previously been shown to have disulfide reductase activity (Leary et al., 2009; Morgada et al., 2015). Consistent with the idea that COA6 potentiates SCO1 function and functionally overlaps with SCO2 to some degree, we found that overexpressing COA6 in *SCO1* and *SCO2* patient cell lines partially rescues CcO activity and COX2 levels (Figures S6A and S6B).

DISCUSSION

A large body of data has established that Cu insertion in the evolutionarily conserved binuclear Cu_A center of CcO occurs in the mitochondrial IMS (Baker et al., 2017; Timón-Gómez et al., 2018). Catalyzing the necessary biochemical reactions in this sub-mitochondrial compartment poses two challenges. First, the Cu-coordinating cysteines of COX2 must be re-reduced to the dithiol form if they become oxidized to disulfides in the oxidizing environment of the IMS. Second, the Cu metallochaperone responsible for delivering Cu to the Cu_A site must be present in the IMS with its Cu-coordinating thiols kept in the reduced state in order to bind Cu ions. Thus, Cu_A assembly is necessarily a two-step process that involves reducing the disulfides of newly synthesized apoCOX2 followed by Cu transfer from a metallochaperone. Here, we show that COA6 is a CHCH domain-containing protein that facilitates Cu_A site maturation by exhibiting disulfide reductase activity toward apo- COX2 and SCO1, the metallochaperone that delivers Cu to reduced apoCOX2. Thus, COA6 likely plays a dual role in Cu_A site maturation by maintaining the Cu-coordinating cysteines of COX2 and its metallochaperone SCO1 in the thiol/thiolate oxidation state to allow for Cu binding.

We have recently shown that metallation of the Cu_A site can be achieved *in vitro* by the combined action of SCO1 and SCO2 proteins, where SCO1 acts as a metallochaperone to transfer two Cu(I) equivalents to COX2 after SCO2 has reduced its cysteine

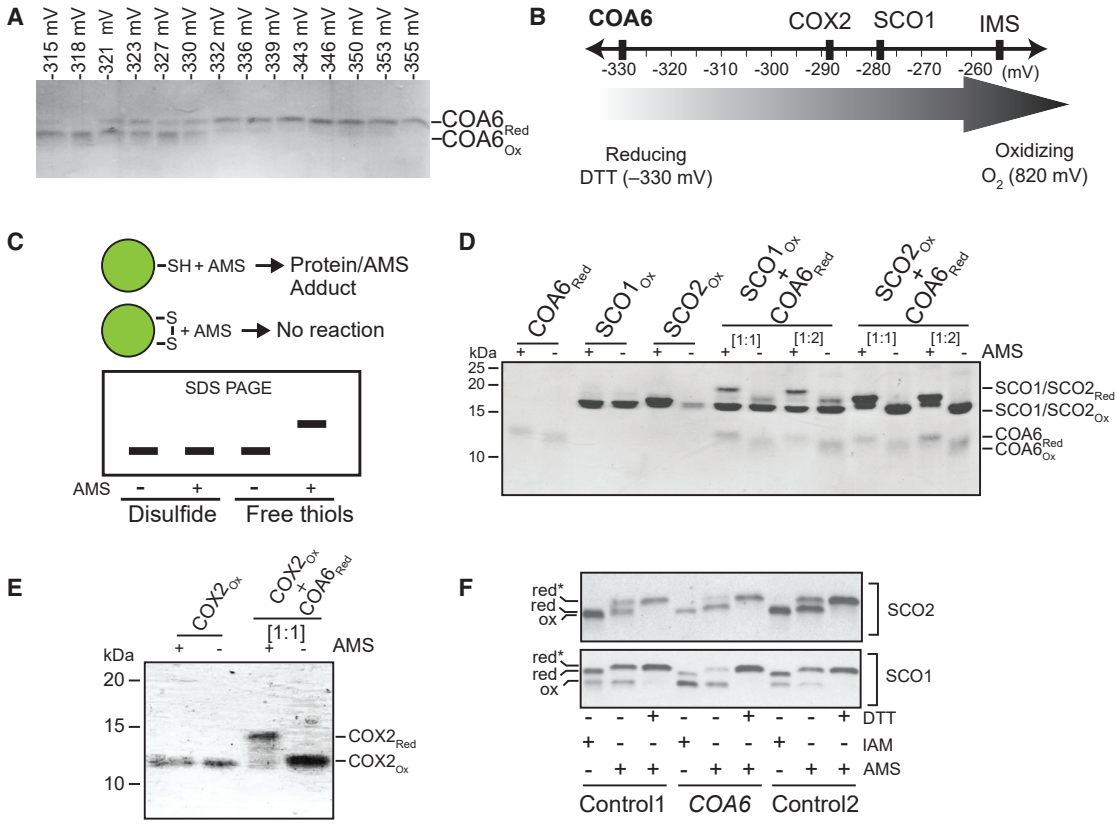

Figure 6. COA6 Acts as a Thiol-Disulfide Reductase of SCO and COX2 Proteins

(A) Determination of the redox potential of recombinant human COA6 by subjecting it to increasing dithiothreitol (DTT) concentrations followed by treatment with the alkylating agent AMS to irreversibly modify cysteines containing reduced thiols. Oxidized and reduced species of COA6 were resolved by non-reducing SDS-PAGE.

(B) Schematic representation of the redox potential of COA6 relative to the previously determined redox potentials of COX2, SCO1, and the mitochondrial intermembrane space (IMS).

(C) A schematic of how AMS reacts with reduced protein thiols resulting in protein-AMS adducts of increased mass and with retarded migration in SDS-PAGE gels under non-reducing conditions.

(D and E) Migration patterns of purified recombinant human COA6, SCO1, and SCO2 (D) and COX2 (E) proteins with and without AMS treatment on non-reducing SDS-PAGE. 1-h co-incubation of reduced COA6 with oxidized SCO1, SCO2, or COX2 was followed by AMS treatment and SDS-PAGE. SCO and COA6 proteins were used at 1:1 and 1:2 stoichiometries. COX2 and COA6 proteins were used at a 1:1 stoichiometry.

(F) Isolated human mitochondria from control (control 1 and control 2) and *COA6* patient fibroblasts were incubated in the presence or absence of the reductant dithiothreitol (DTT), followed by treatment with the alkylating agents iodoacetamide (IAM) or AMS to irreversibly modify cysteines containing reduced thiols. Species of SCO1 and SCO2 containing oxidized (ox) cysteines were then resolved from those with reduced (red) cysteines by non-reducing SDS-PAGE and detected by immunoblotting with the indicated antibodies. Red* refers to reduced thiols that were modified in the presence of AMS. These data are representative of three independent replicates.

residues to render it competent for Cu binding (Morgada et al., 2015). While the two orthologous SCO proteins thus are sufficient to form the Cu_A center *in vitro*, genetic and protein-protein interaction data all argue that the final step in the metallation of Cu_A site requires the combined activities of at least three proteins: SCO1, SCO2, and COA6 (Ghosh et al., 2016; Pacheu-Grau et al., 2015; Stroud et al., 2015). To address the discrepancy between the *in vitro* and *in vivo* data, we decided to focus on determining the function of COA6, the most recently discovered member of this Cu delivery pathway.

The fact that human COA6 is a small, soluble protein makes it highly amenable to NMR-based structure determination. Thus, we utilized NMR to solve the solution structure of COA6 and identify a CHCH domain (Figure 1F). Consistent with our studies, Maghool et al. (2019) recently published the X-ray crystallographic structure of a COA6 dimer while we were revising our article, showing that each COA6 monomer has a CHCH fold with the first two helices being stabilized by disulfide bonds. The presence of COA6 as a dimer both *in vitro* (Figure 1C) and *in vivo* (Figures 5A and 5C) suggests that dimerization may be physiologically significant. Based on our observations that the COA6 dimer is readily disrupted in the presence of either SCO protein and binds to SCO proteins as a monomer (Figure 3), we speculate that COA6 dimerization *in vivo* may prevent its non-specific activity against other mitochondrial intermembrane space proteins. The CHCH domain identified in COA6 has been

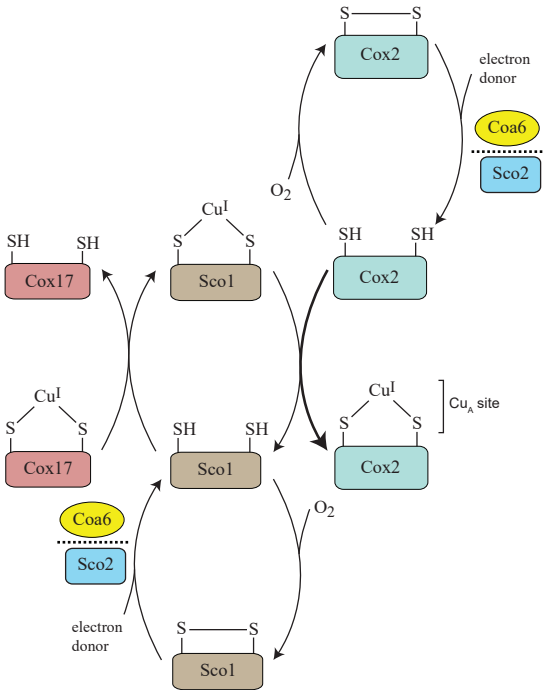

Figure 7. A Proposed Model of Cu_A Site Biogenesis

Cu_A site formation on the Cox2 subunit of CcO involves sequential transfer of Cu from Cox17 to Sco1 to Cox2. This process occurs in the mitochondrial inter-membrane space, an oxidizing environment that would promote the formation of disulfide bonds in the Cu-coordinating cysteines of apo-Cox2 and apo-Sco1 proteins and prevent Cu binding. The thioldisulfide oxidoreductase activities of Coa6 and Sco2 overcome this problem by reducing the disulfides of apo-Cox2 and apo-Sco1 to dithiols, thereby allowing for Cu binding. Previous studies and the work described here suggest that Coa6 has dual substrates in Sco1 and Cox2 and that it exhibits overlapping substrate specificity with Sco2.

proposed to be the minimal domain require for thiol-disulfide oxidoreductase activity (Banci et al., 2009a). We found that COA6 function can be bypassed under reducing or hypoxic conditions (Figures 5E–5G), suggesting that it may exhibit disulfide reductase activity. Indeed, our *in vitro* and *in vivo* experiments further support this notion and identified SCO1 and COX2 as COA6 client proteins (Figures 3 and 6). Having two client proteins for a disulfide reductase is not without precedent; the bacterial periplasmic protein thioredoxin TlpA acts as a specific reductant for both of the metallochaperones SCO1 and COXB, the bacterial equivalent of COX2 (Abicht et al., 2014; Mohorko et al., 2012). Thus, COA6 appears to be a functional homolog of bacterial TlpA; however, it likely represents a product of convergent evolution, as there is no sequence homology between the two proteins. We propose that the client-specific disulfide reductases in the bacterial periplasmic space and the mitochondrial IMS are required to counter the oxidizing environment of these compartments, which would prevent Cu coordination by promoting disulfide bond formation in the Cu-binding proteins (Herrmann et al., 2009).

Our findings beg the question why three proteins—COA6, SCO1, and SCO2—are needed *in vivo* when SCO1 and SCO2 are sufficient to form a Cu_A center *in vitro*. The redox states of SCO1 and SCO2 *in vitro* were set to favor Cu delivery to the Cu_A site (Morgada et al., 2015). *In vivo*, however, the reduced states of these proteins must be continuously regenerated for the proteins to function. Thus, after delivering Cu to the Cu_A site, the cysteines of SCO1 are likely to be more prone to oxidation given the oxidizing nature of the mitochondrial IMS, necessitating their subsequent reduction to bind Cu for the next round of Cu delivery to apoCOX2. In this setting, COA6 function may be critical. Previously, it was shown that the metallochaperone COX17 is capable of transferring both reducing equivalents and Cu to SCO1 *in vitro*, although the redox potential of the S-S/2SH redox couple of COX17 (−198 mV) is not thermodynamically favored to reduce the disulfide of SCO1 (−277 mV) (Banci et al., 2008) but a Cu-bound COX17 is able to overcome unfavorable thermodynamic driving force *in vitro*. Based on these observations and our findings, it appears that COA6 is a more likely electron donor for SCO1 *in vivo*.

By combining both *in vivo* and *in vitro* approaches, our study demonstrates that the mechanism of mitochondrial Cu_A site biogenesis requires the combined activities of COA6, SCO1, and SCO2, with COA6 facilitating Cu delivery to the Cu_A site by keeping the Cu-binding cysteines of SCO1 and COX2 in their reduced states (Figure 7). This model raises an obvious question regarding the ultimate source of the reducing power. Although at present this remains unknown, our model is consistent with the previously documented synthetic lethal interaction between *coa6Δ* and *sco2Δ* yeast mutants (Ghosh et al., 2016), in that both COA6 and SCO2 exhibit disulfide reductase activities with some overlapping substrate specificity in SCO1 and/or COX2 (Figure 7). Our structural model of the COA6:SCO1 complex (Figure 4E) suggests a possible redox pathway for shuttling electrons from COA6 to the Cu-binding cysteines of SCO1 (Cys 169 and Cys173). Both Cys169 and Cys173 are in close proximity to the indole ring of W48 from COA6, which is also within 5 Å of the Cys12/Cys44 disulfide bridge of COA6. We propose that the polarizable π electrons of the W48 indole ring could help relay the transfer of electrons between Cys12/Cys44 (of COA6) and Cys169/Cys173 (of SCO1) as a possible mechanism of the observed COA6 disulfide reductase activity. We further suggest that the other COA6 disulfide bridge (Cys22/Cys33) may similarly help catalyze the reduction of disulfides in COX2. In this scenario, a ternary complex of COA6 bound to both SCO1 and COX2 could simultaneously promote Cu binding to both SCO1 and COX2. This model is supported by our previous study, which showed that a pathogenic mutation in the first tryptophan residue of COA6 disrupts its ability to interact with COX2 but not with SCO1, indicating that COA6 uses distinct surfaces to interact with each protein (Ghosh et al., 2016). Additional support for our model comes from a recent report, which identified a SCO1-COA6-COX2 assembly module in yeast CcO biogenesis (Franco et al., 2018). In summary, our work provides structural, biochemical, and *in vivo* data supporting the role of COA6 as a disulfide reductase in the IMS and advances the mechanistic model of Cu_A site assembly within the complex picture of CcO biogenesis.

STAR★METHODS

Detailed methods are provided in the online version of this paper and include the following:

- KEY RESOURCES TABLE
- LEAD CONTACT AND MATERIALS AVAILABILITY
- EXPERIMENTAL MODEL AND SUBJECT DETAILS
  - Yeast Strains and Culture Conditions
  - Mammalian Cell Culture
- METHOD DETAILS
  - Cloning and Expression
  - Protein Purification
  - NMR Spectroscopy
  - Relaxation Measurements
  - Online Liquid Chromatography-Inductively Coupled Plasma-Mass Spectrometry (LC-ICP-MS)
  - Gel-Filtration Chromatography
  - Haddock Docking Calculation of the COA6:SCO1 Complex
  - SDS-PAGE and Western Blotting
  - CcO Activity
  - Redox State Determination
  - Reduction Potential Determination
  - *In Vitro* Labeling of Mitochondrial Translation Products
- QUANTIFICATION AND STATISTICAL ANALYSIS
- DATA AND CODE AVAILABILITY

SUPPLEMENTAL INFORMATION

Supplemental Information can be found online at https://doi.org/10.1016/j.celrep.2019.11.054.

ACKNOWLEDGMENTS

Research reported in this publication was supported by NIH awards R01GM111672 to V.M.G., R35GM127021 to P.A.L., and R01EY012347 to J.B.A. This work was further supported by Welch Foundation grant A-1810 to V.M.G., a T3 grant from Texas A&M University to V.M.G. and P.A.L., and a Canadian Institutes of Health Research Operating grant (MOP 133562) to S.C.L. A.J.V. is a CONICET staff member and M.N.M. is a recipient of a post-doctoral fellowship from CONICET. The content is solely the responsibility of the authors and does not necessarily represent the official views of the NIH.

AUTHOR CONTRIBUTIONS

V.M.G. and A.J.V. conceptualized the project. V.M.G., A.J.V., S.C.L., P.A.L., and M.T.N. designed the experiments. S.S., M.N.M., M.T.N., A.B., A.A.R., N.D., and A.G. performed the experiments. S.S., M.N.M., M.T.N, A.B., A.A.R., N.D., Q.Y., and J.B.A. analyzed the data. V.M.G., A.J.V., S.S., M.N.M., M.T.N., S.C.L., and P.A.L. wrote the manuscript. V.M.G., A.J.V., S.C.L., P.A.L., and J.B.A. were responsible for the resources and funding acquisition, and V.M.G. coordinated the whole project.

DECLARATION OF INTERESTS

The authors declare no competing interests.

Received: July 3, 2019
Revised: October 7, 2019
Accepted: November 13, 2019
Published: December 17, 2019

SUPPORTING CITATIONS

The following reference appears in the Supplemental Information: Rebelo et al., 2018.

REFERENCES

Abajian, C., and Rosenzweig, A.C. (2006). Crystal structure of yeast Sco1. J. Biol. Inorg. Chem. *11*, 459–466.

Abajian, C., Yatsunyk, L.A., Ramirez, B.E., and Rosenzweig, A.C. (2004). Yeast cox17 solution structure and Copper(I) binding. J. Biol. Chem. *279*, 53584–53592.

Abicht, H.K., Schärer, M.A., Quade, N., Ledermann, R., Mohorko, E., Capitani, G., Hennecke, H., and Glockshuber, R. (2014). How periplasmic thioredoxin TlpA reduces bacterial copper chaperone ScoI and cytochrome oxidase subunit II (CoxB) prior to metallation. J. Biol. Chem. *289*, 32431–32444.

Abriata, L.A., Banci, L., Bertini, I., Ciofi-Baffoni, S., Gkazonis, P., Spyroulias, G.A., Vila, A.J., and Wang, S. (2008). Mechanism of Cu(A) assembly. Nat. Chem. Biol. *4*, 599–601.

Baertling, F., A M van den Brand, M., Hertecant, J.L., Al-Shamsi, A., P van den Heuvel, L., Distelmaier, F., Mayatepek, E., Smeitink, J.A., Nijtmans, L.G., and Rodenburg, R.J. (2015). Mutations in COA6 cause cytochrome c oxidase deficiency and neonatal hypertrophic cardiomyopathy. Hum. Mutat. *36*, 34–38.

Baker, Z.N., Cobine, P.A., and Leary, S.C. (2017). The mitochondrion: a central architect of copper homeostasis. Metallomics *9*, 1501–1512.

Banci, L., Bertini, I., Calderone, V., Ciofi-Baffoni, S., Mangani, S., Martinelli, M., Palumaa, P., and Wang, S. (2006). A hint for the function of human Sco1 from different structures. Proc. Natl. Acad. Sci. USA *103*, 8595–8600.

Banci, L., Bertini, I., Ciofi-Baffoni, S., Gerothanassis, I.P., Leontari, I., Martinelli, M., and Wang, S. (2007). A structural characterization of human SCO2. Structure *15*, 1132–1140.

Banci, L., Bertini, I., Ciofi-Baffoni, S., Hadjiloi, T., Martinelli, M., and Palumaa, P. (2008). Mitochondrial copper(I) transfer from Cox17 to Sco1 is coupled to electron transfer. Proc. Natl. Acad. Sci. USA *105*, 6803–6808.

Banci, L., Bertini, I., Cefaro, C., Ciofi-Baffoni, S., Gallo, A., Martinelli, M., Sideris, D.P., Katrakili, N., and Tokatlidis, K. (2009a). MIA40 is an oxidoreductase that catalyzes oxidative protein folding in mitochondria. Nat. Struct. Mol. Biol. *16*, 198–206.

Banci, L., Bertini, I., Ciofi-Baffoni, S., and Tokatlidis, K. (2009b). The coiled coil-helix-coiled coil-helix proteins may be redox proteins. FEBS Lett. *583*, 1699–1702.

Bhattacharya, A., Tejero, R., and Montelione, G.T. (2007). Evaluating protein structures determined by structural genomics consortia. Proteins *66*, 778–795.

Bihlmaier, K., Mesecke, N., Terziyska, N., Bien, M., Hell, K., and Herrmann, J.M. (2007). The disulfide relay system of mitochondria is connected to the respiratory chain. J. Cell Biol. *179*, 389–395.

Boulet, A., Vest, K.E., Maynard, M.K., Gammon, M.G., Russell, A.C., Mathews, A.T., Cole, S.E., Zhu, X., Phillips, C.B., Kwong, J.Q., et al. (2018). The mammalian phosphate carrier SLC25A3 is a mitochondrial copper transporter required for cytochrome *c* oxidase biogenesis. J. Biol. Chem. *293*, 1887–1896.

Bourens, M., Boulet, A., Leary, S.C., and Barrientos, A. (2014). Human COX20 cooperates with SCO1 and SCO2 to mature COX2 and promote the assembly of cytochrome c oxidase. Hum. Mol. Genet. *23*, 2901–2913.

Calvo, S.E., Compton, A.G., Hershman, S.G., Lim, S.C., Lieber, D.S., Tucker, E.J., Laskowski, A., Garone, C., Liu, S., Jaffe, D.B., et al. (2012). Molecular diagnosis of infantile mitochondrial disease with targeted next-generation sequencing. Sci. Transl. Med. *4*, 118ra10.

Capaldi, R.A., Marusich, M.F., and Taanman, J.W. (1995). Mammalian cytochrome-c oxidase: characterization of enzyme and immunological detection of subunits in tissue extracts and whole cells. Methods Enzymol. *260*, 117–132.

Cobine, P.A., Pierrel, F., Leary, S.C., Sasarman, F., Horng, Y.C., Shoubridge, E.A., and Winge, D.R. (2006). The P174L mutation in human Sco1 severely compromises Cox17-dependent metallation but does not impair copper binding. J. Biol. Chem. *281*, 12270–12276.

de Vries, S.J., van Dijk, M., and Bonvin, A.M. (2010). The HADDOCK web server for data-driven biomolecular docking. Nat. Protoc. *5*, 883–897.

Dziuba, N., Hardy, J., and Lindahl, P.A. (2018). Low-molecular-mass iron in healthy blood plasma is not predominately ferric citrate. Metallomics *10*, 802–817.

Ferguson-Miller, S., and Babcock, G.T. (1996). Heme/Copper Terminal Oxidases. Chem. Rev. *96*, 2889–2908.

Foster, A.W., Osman, D., and Robinson, N.J. (2014). Metal preferences and metallation. J. Biol. Chem. *289*, 28095–28103.

Franco, L.V.R., Su, C.H., McStay, G.P., Yu, G.J., and Tzagoloff, A. (2018). Cox2p of yeast cytochrome oxidase assembles as a stand-alone subunit with the Cox1p and Cox3p modules. J. Biol. Chem. *293*, 16899–16911.

Ghosh, A., Trivedi, P.P., Timbalia, S.A., Griffin, A.T., Rahn, J.J., Chan, S.S., and Gohil, V.M. (2014). Copper supplementation restores cytochrome c oxidase assembly defect in a mitochondrial disease model of COA6 deficiency. Hum. Mol. Genet. *23*, 3596–3606.

Ghosh, A., Pratt, A.T., Soma, S., Theriault, S.G., Griffin, A.T., Trivedi, P.P., and Gohil, V.M. (2016). Mitochondrial disease genes COA6, COX6B and SCO2 have overlapping roles in COX2 biogenesis. Hum. Mol. Genet. *25*, 660–671.

Güntert, P., and Buchner, L. (2015). Combined automated NOE assignment and structure calculation with CYANA. J. Biomol. NMR *62*, 453–471.

Güntert, P., Mumenthaler, C., and Wüthrich, K. (1997). Torsion angle dynamics for NMR structure calculation with the new program DYANA. J. Mol. Biol. *273*, 283–298.

Halliwell, B., and Gutteridge, J.M. (1984). Oxygen toxicity, oxygen radicals, transition metals and disease. Biochem. J. *219*, 1–14.

Herrmann, J.M., Kauff, F., and Neuhaus, H.E. (2009). Thiol oxidation in bacteria, mitochondria and chloroplasts: common principles but three unrelated machineries? Biochim. Biophys. Acta *1793*, 71–77.

Horng, Y.C., Cobine, P.A., Maxfield, A.B., Carr, H.S., and Winge, D.R. (2004). Specific copper transfer from the Cox17 metallochaperone to both Sco1 and Cox11 in the assembly of yeast cytochrome C oxidase. J. Biol. Chem. *279*, 35334–35340.

Hu, J., Dong, L., and Outten, C.E. (2008). The redox environment in the mitochondrial intermembrane space is maintained separately from the cytosol and matrix. J. Biol. Chem. *283*, 29126–29134.

Kim, B.E., Nevitt, T., and Thiele, D.J. (2008). Mechanisms for copper acquisition, distribution and regulation. Nat. Chem. Biol. *4*, 176–185.

Leary, S.C., and Sasarman, F. (2009). Oxidative phosphorylation: synthesis of mitochondrially encoded proteins and assembly of individual structural subunits into functional holoenzyme complexes. Methods Mol. Biol. *554*, 143–162.

Leary, S.C., Kaufman, B.A., Pellecchia, G., Guercin, G.H., Mattman, A., Jaksch, M., and Shoubridge, E.A. (2004). Human SCO1 and SCO2 have independent, cooperative functions in copper delivery to cytochrome c oxidase. Hum. Mol. Genet. *13*, 1839–1848.

Leary, S.C., Sasarman, F., Nishimura, T., and Shoubridge, E.A. (2009). Human SCO2 is required for the synthesis of CO II and as a thiol-disulphide oxidoreductase for SCO1. Hum. Mol. Genet. *18*, 2230–2240.

Leary, S.C., Antonicka, H., Sasarman, F., Weraarpachai, W., Cobine, P.A., Pan, M., Brown, G.K., Brown, R., Majewski, J., Ha, K.C., et al. (2013). Novel mutations in SCO1 as a cause of fatal infantile encephalopathy and lactic acidosis. Hum. Mutat. *34*, 1366–1370.

Macomber, L., and Imlay, J.A. (2009). The iron-sulfur clusters of dehydratases are primary intracellular targets of copper toxicity. Proc. Natl. Acad. Sci. USA *106*, 8344–8349.

Maghool, S., Cooray, N.D.G., Stroud, D.A., Aragão, D., Ryan, M.T., and Maher, M.J. (2019). Structural and functional characterization of the mitochondrial complex IV assembly factor Coa6. Life Sci. Alliance *2*, e201900458.

Markley, J.L., Bax, A., Arata, Y., Hilbers, C.W., Kaptein, R., Sykes, B.D., Wright, P.E., and Wüthrich, K.; IUPAC-IUBMB-IUPAB Inter-Union Task Group on the Standardization of Data Bases of Protein and Nucleic Acid Structures Determined by NMR Spectroscopy (1998). Recommendations for the presentation of NMR structures of proteins and nucleic acids. J. Biomol. NMR *12*, 1–23.

Mohorko, E., Abicht, H.K., Bühler, D., Glockshuber, R., Hennecke, H., and Fischer, H.M. (2012). Thioredoxin-like protein TlpA from Bradyrhizobium japonicum is a reductant for the copper metallochaperone ScoI. FEBS Lett. *586*, 4094–4099.

Morgada, M.N., Abriata, L.A., Cefaro, C., Gajda, K., Banci, L., and Vila, A.J. (2015). Loop recognition and copper-mediated disulfide reduction underpin metal site assembly of CuA in human cytochrome oxidase. Proc. Natl. Acad. Sci. USA *112*, 11771–11776.

Nguyen, T.Q., Dziuba, N., and Lindahl, P.A. (2019). Isolated Saccharomyces cerevisiae vacuoles contain low-molecular-mass transition-metal polyphosphate complexes. Metallomics *11*, 1298–1309.

Pacheu-Grau, D., Bareth, B., Dudek, J., Juris, L., Vögtle, F.N., Wissel, M., Leary, S.C., Dennerlein, S., Rehling, P., and Deckers, M. (2015). Cooperation between COA6 and SCO2 in COX2 maturation during cytochrome c oxidase assembly links two mitochondrial cardiomyopathies. Cell Metab. *21*, 823–833.

Papadopoulou, L.C., Sue, C.M., Davidson, M.M., Tanji, K., Nishino, I., Sadlock, J.E., Krishna, S., Walker, W., Selby, J., Glerum, D.M., et al. (1999). Fatal infantile cardioencephalomyopathy with COX deficiency and mutations in SCO2, a COX assembly gene. Nat. Genet. *23*, 333–337.

Rebelo, A.P., Saade, D., Pereira, C.V., Farooq, A., Huff, T.C., Abreu, L., Moraes, C.T., Mnatsakanova, D., Mathews, K., Yang, H., et al. (2018). SCO2 mutations cause early-onset axonal Charcot-Marie-Tooth disease associated with cellular copper deficiency. Brain *141*, 662–672.

Schwieters, C.D., Kuszewski, J.J., Tjandra, N., and Clore, G.M. (2003). The Xplor-NIH NMR molecular structure determination package. J. Magn. Reson. *160*, 65–73.

Sharma, D., and Rajarathnam, K. (2000). 13C NMR chemical shifts can predict disulfide bond formation. J. Biomol. NMR *18*, 165–171.

Shen, Y., Delaglio, F., Cornilescu, G., and Bax, A. (2009). TALOS+: a hybrid method for predicting protein backbone torsion angles from NMR chemical shifts. J. Biomol. NMR *44*, 213–223.

Soma, S., Latimer, A.J., Chun, H., Vicary, A.C., Timbalia, S.A., Boulet, A., Rahn, J.J., Chan, S.S.L., Leary, S.C., Kim, B.E., et al. (2018). Elesclomol restores mitochondrial function in genetic models of copper deficiency. Proc. Natl. Acad. Sci. USA *115*, 8161–8166.

Soto, I.C., Fontanesi, F., Liu, J., and Barrientos, A. (2012). Biogenesis and assembly of eukaryotic cytochrome c oxidase catalytic core. Biochim. Biophys. Acta *1817*, 883–897.

Stiburek, L., Vesela, K., Hansikova, H., Hulkova, H., and Zeman, J. (2009). Loss of function of Sco1 and its interaction with cytochrome c oxidase. Am. J. Physiol. Cell Physiol. *296*, C1218–C1226.

Stroud, D.A., Maher, M.J., Lindau, C., Vögtle, F.N., Frazier, A.E., Surgenor, E., Mountford, H., Singh, A.P., Bonas, M., Oeljeklaus, S., et al. (2015). COA6 is a mitochondrial complex IV assembly factor critical for biogenesis of mtDNA-encoded COX2. Hum. Mol. Genet. *24*, 5404–5415.

Timón-Gómez, A., Nývltová, E., Abriata, L.A., Vila, A.J., Hosler, J., and Barrientos, A. (2018). Mitochondrial cytochrome c oxidase biogenesis: Recent developments. Semin. Cell Dev. Biol. *76*, 163–178.

Tsukihara, T., Aoyama, H., Yamashita, E., Tomizaki, T., Yamaguchi, H., Shinzawa-Itoh, K., Nakashima, R., Yaono, R., and Yoshikawa, S. (1995). Structures of metal sites of oxidized bovine heart cytochrome c oxidase at 2.8 A. Science *269*, 1069–1074.

Valnot, I., Osmond, S., Gigarel, N., Mehaye, B., Amiel, J., Cormier-Daire, V., Munnich, A., Bonnefont, J.P., Rustin, P., and Rötig, A. (2000). Mutations of

the SCO1 gene in mitochondrial cytochrome c oxidase deficiency with neonatal-onset hepatic failure and encephalopathy. Am. J. Hum. Genet. *67*, 1104–1109.

van Zundert, G.C., and Bonvin, A.M. (2014). Modeling protein-protein complexes using the HADDOCK webserver "modeling protein complexes with HADDOCK". Methods Mol. Biol. *1137*, 163–179.

Vögtle, F.N., Burkhart, J.M., Gonczarowska-Jorge, H., Kücükköse, C., Taskin, A.A., Kopczynski, D., Ahrends, R., Mossmann, D., Sickmann, A., Zahedi, R.P., and Meisinger, C. (2017). Landscape of submitochondrial protein distribution. Nat. Commun. *8*, 290.

Williamson, M.P., Havel, T.F., and Wüthrich, K. (1985). Solution conformation of proteinase inhibitor IIA from bull seminal plasma by 1H nuclear magnetic resonance and distance geometry. J. Mol. Biol. *182*, 295–315.

Wishart, D.S., and Sykes, B.D. (1994). The 13C chemical-shift index: a simple method for the identification of protein secondary structure using 13C chemical-shift data. J. Biomol. NMR *4*, 171–180.

STAR★METHODS

KEY RESOURCES TABLE

REAGENT or RESOURCE	SOURCE	IDENTIFIER
Antibodies		
Mouse monoclonal anti-Por1	Abcam	Cat# ab110326; RRID:AB_10865182
Mouse monoclonal anti-Cox2	Abcam	Cat# ab110271; RRID:AB_10858117
Rabbit polyclonal anti-Coa6	Gohil Lab	N/A
Rabbit polyclonal anti- SCO1	Bourens et al., 2014	N/A
Rabbit polyclonal anti- SCO2	Fitzgerald	Cat# 70R-20118
Rabbit Polyclonal anti- COA6	Proteintech	Cat# 24209-1-AP
Mouse monoclonal anti- COX2	Mitoscience	Cat# MS405; RRID:AB_1618186
Rabbit monoclonal anti- GAPDH	Cell signaling	Cat# 14C10-2118
hFAB Rhodamine anti-Actin	Bio-Rad	Cat# 12004163
Bacterial and Virus Strains		
E. coli strain DH5α	NEB	Cat# C2987I
E. coli BL21(DE3)	NEB	Cat# C2527I
Chemicals, Peptides, and Recombinant Proteins		
Ammonium-^{15}N chloride	Sigma-Aldrich	Cat# 299251
BME Vitamins 100x solution	Sigma-Aldrich	Cat# B6891
D-(+)-Raffinose pentahydrate	Sigma-Aldrich	Cat# R0250
D-Glucose-$^{13}C_6$	Sigma-Aldrich	Cat# 389374
DL-Dithiothreitol	Sigma-Aldrich	Cat# D0632
Ergosterol	Sigma-Aldrich	Cat# 45480
Isopropyl β-D-thiogalactoside	Sigma-Aldrich	Cat# I6758
Trans-4,5-Dihydroxy-1,2-dithiane (Oxidized DTT)	Sigma-Aldrich	Cat# D3511
Deposited Data		
Human COA6 structure	This Paper	PDB: 6NL3
Experimental Models: Cell Lines		
COA6 patient cell line	Baertling et al., 2015	N/A
SCO1-1 (R149X/P174L) patient cell line	Valnot et al., 2000	N/A
SCO1-2 (V93X/M294V) patient cell line	Leary et al., 2013	N/A
SCO2-9 patient cell line	Leary et al., 2013	N/A
Experimental Models: Organisms/Strains		
S. cerevisiae: Strain background: BY4741 WT - *MATa, his3Δ1, leu2Δ0, met15Δ0, ura3Δ0*	Miriam L. Greenberg	N/A
S. cerevisiae: Strain background: BY4741 *coa6Δ - MATa, his3Δ1, leu2Δ0, met15Δ0, ura3Δ0 coa6Δ::kanMX4*	Open Biosystems	N/A
S. cerevisiae: Strain background: BY4741 *sco1Δ - MATa, his3Δ1, leu2Δ0, met15Δ0, ura3Δ0 sco1Δ::kanMX4*	Open Biosystems	N/A
S. cerevisiae: Strain background: BY4741 *sco2Δ - MATa, his3Δ1, leu2Δ0, met15Δ0, ura3Δ0 sco2Δ::kanMX4*	Open Biosystems	N/A
S. cerevisiae: Strain background: BY4741 *cox11Δ - MATa, his3Δ1, leu2Δ0, met15Δ0, ura3Δ0 cox11Δ::kanMX4*	Open Biosystems	N/A

(*Continued on next page*)

Continued

REAGENT or RESOURCE	SOURCE	IDENTIFIER
S. cerevisiae: Strain background: BY4741 *cox17Δ - MATa, his3Δ1, leu2Δ0, met15Δ0, ura3Δ0 cox17Δ::kanMX4*	Open Biosystems	N/A
S. cerevisiae: Strain background: STY10 *sco2Δcoa6Δ - MATa, his3Δ1, leu2Δ0, ura3Δ0, lys2Δ0, sco2Δ::KanMX4, coa6Δ::NatMX4*	Ghosh et al., 2016	N/A
Recombinant DNA		
pGEX4t-1- COA6 isoform3	This paper	N/A
pET28a- Coa6	This paper	N/A
pETG-30A- SCO1	Banci et al., 2006	N/A
pETG-30A- SCO2	Banci et al., 2007	N/A
pET9a-COX2-chimeric protein	Morgada et al., 2015	N/A
pRS416 –hyCOA6	Ghosh et al., 2016	N/A
pRS416 –hyCOA6$_{W26C}$	Soma et al., 2018	N/A
pRS416 –hyCOA6$_{W33R}$	Soma et al., 2018	N/A
pRS416 –hyCOA6$_{E54X}$	Soma et al., 2018	N/A
pRS416 –hyCOA6(Δ65-79)	This paper	N/A
pRS416 –hyCOA6(Δ73-79)	This paper	N/A
Software and Algorithms		
The PyMOL Molecular Graphics System, v2.0	Schrödinger LLC	https://pymol.org/2/
HADDOCK2.2	van Zundert and Bonvin, 2014	http://haddock.science.uu.nl/services/HADDOCK2.2/
Topspin, version 3.2	Bruker, Germany	N/A
Sparky, version 3.112	UCSF	https://www.cgl.ucsf.edu/home/sparky/distrib-3.112/download.html
CYANA software package	Güntert and Buchner, 2015	https://www.las.jp/english/products/cyana.html
TALOS+	Shen et al., 2009	https://spin.niddk.nih.gov/bax/nmrserver/talos/
Xplor NIH version 2.50	Schwieters et al., 2003	https://nmr.cit.nih.gov/xplor-nih/
Protein Structure Validation Software suite 1.5	Bhattacharya et al., 2007	https://psvs-1_5-dev.nesg.org/

LEAD CONTACT AND MATERIALS AVAILABILITY

Further information and requests for resources and reagents should be directed to and will be fulfilled by the Lead Contact, Vishal M. Gohil (vgohil@tamu.edu). All unique/stable reagents generated in this study are available from the Lead Contact without restrictions.

EXPERIMENTAL MODEL AND SUBJECT DETAILS

Yeast Strains and Culture Conditions

All strains used in this study are listed in the Key Resources Table, and all the primers used in this study are listed in Table S2. Yeast cells were grown in YP (1% yeast extract, 2% bactopeptone) medium with 2% dextrose (YPD) or 3% glycerol + 1% ethanol (YPGE) as carbon sources. Synthetic media was prepared with 0.17% yeast nitrogen base, 0.5% ammonium sulfate, 0.2% dropout amino acid mix and 2% dextrose as a carbon source. Solid media was prepared by further adding 2% agar. Growth was measured spectrophotometrically at 600 nm in liquid medium or by spotting on solid plates. For hypoxic growth conditions on solid media, indicated plates were incubated in a hypoxia incubator chamber (STEMCELL Technologies) purged with a certified gas mixture (4% oxygen, 5% carbon dioxide and 91% nitrogen). For hypoxic growth conditions in liquid media, synthetic complete raffinose liquid media, which constitutes 2% raffinose and 1x TEM (0.5% Tween80, 2.4 μg/ml ergosterol, 55.6 μg/ml methionine), was kept in a glove box with nitrogen gas for 24 hr prior to culturing the indicated strains at 30°C while shaking at 225 rpm.

Mammalian Cell Culture

Primary fibroblasts from control, *COA6* (Baertling et al., 2015), *SCO1-1* (R149X/P174L; Valnot et al., 2000), *SCO1-2* (V93X/M294V; Leary et al., 2013) and *SCO2-9* (Leary et al., 2013) were immortalized as described (Leary et al., 2004). Fibroblasts were transduced at 40%–60% confluency with retrovirus produced by the Phoenix amphotrophic packaging cell line, and selected in media containing

hygromycin or puromycin to yield stable overexpression cell lines (Leary et al., 2004). Both fibroblasts and the packaging cells were grown in high-glucose DMEM containing 10% bovine growth serum (ThermoFisher) at 37°C in 5% CO_2 and were tested to ensure that they were *Mycoplasma*-free (Lonza MycoAlert) before harvesting.

METHOD DETAILS

Cloning and Expression

E.coli codon optimized human *COA6* isoform3 was cloned into the pGEX4t-1 vector using BamHI and XhoI restriction endonucleases to generate N-terminal, GST-fused *COA6*. *E.coli* codon optimized yeast *COA6* was cloned into the pET28a plasmid using XhoI and EcoRI restriction endonucleases to generate N-terminal, His-GFP-fused *COA6*. The resultant plasmids were then transformed into *E.coli* BL 21(DE3) cells. Human COA6 and yeast Coa6 expression was induced by the addition of 0.5 mM isopropyl-D-thiogalactopyranoside (IPTG) at an optical density of 600 nm (OD_{600}) of 0.6, and the cells were grown at 37°C and 16°C for 4 hr and 12 hr respectively. $^{15}N/^{13}C$ labeled proteins for NMR structural characterization were expressed in cells grown in minimal medium, which contained 3 g/liter KH_2PO_4, 6.8 g/liter Na_2HPO_4, 0.1 mM $CaCl_2$, 2 mM $MgCl_2$, 1x Basal Medium Eagle (BME) vitamin solution (Sigma), 1 g/liter ^{15}N-ammonium chloride and 4 g/liter ^{13}C-D-glucose (Sigma).

Protein Purification

To purify human COA6, cells were resuspended in lysis buffer (50 mM Tris [pH 7.4], 150 mM NaCl, 1 mM PMSF and 0.1% Triton X-100) and lysed by repeated sonication on ice for a total of 4 min. The lysate was clarified by centrifugation at 40,000 g for 30 min at 4°C and the supernatant was applied to a GST binding column pre-equilibrated with a buffer containing 50 mM Tris (pH 7.4) and 150 mM NaCl. GST-COA6 was eluted in equilibration buffer supplemented with 10 mM reduced glutathione. Eluted GST-COA6 was subjected to thrombin digestion (20 units of thrombin for 100 mg of GST-COA6 protein) for 12 hr at room temperature. COA6 from the flow-through was then injected into a HiPrep Sephacryl S-100 column pre-equilibrated with a 20 mM Tris (pH 7.4) and 150 mM NaCl solution.

To purify yeast Coa6, cells were resuspended in lysis buffer containing 20 mM Tris (pH 8), 500 mM NaCl, 1 mM PMSF and 6 mM imidazole and sonicated on ice for 4 min. The lysate was clarified by centrifugation at 40,000 g for 30 min at 4°C and the supernatant was applied to a HisTrap HP column pre-equilibrated with 20 mM Tris (pH 8), 500 mM NaCl, and 6mM imidazole. His-GFP-Coa6 was eluted using 20 mM Tris (pH 8), 500 mM NaCl, and 400 mM imidazole. Eluted His-GFP-Coa6 was subjected to TEV digestion for 12 hr at 4°C. Yeast Coa6 was further purified using a Superdex 200 column pre-equilibrated with 20mM Tris (pH 7.4) and 500 mM NaCl. Human SCO1 and SCO2 were purified as described (Banci et al., 2006, 2007).

NMR Spectroscopy

NMR data were acquired in Shigemi tubes on 0.015 – 0.947 mM COA6 samples buffered in 20mM Tris (pH 7.4), 150 mM NaCl and 10% (v/v) D_2O. All NMR experiments used for the structure calculation were carried out at 25°C on the Bruker Avance 800 MHz, 600 MHz, or 500 MHz NMR spectrometers equipped with a 5 mm triple-resonance cryoprobe and single-axis pulsed field gradient by using standard pulse programs provided by the instrument manufacturer. NMR data were acquired and processed by using the software Topspin, version 3.2 (Bruker, Germany), and were further analyzed in Sparky, version 3.112 (University of California, San Francisco).

^1H, ^{13}C, and ^{15}N resonance assignments for Coa6 were indirectly referenced according to the IUPAC recommendations (Markley et al., 1998). The protein backbone resonance assignments were achieved through analysis of the 3D-triple resonance experiments and the aliphatic side-chain resonances were primarily assigned using 3D-HCCH-COSY and ^{15}N-edited TOCSY-HSQC acquired with 60 ms mixing time. Aromatic side-chains were assigned using 2D-homo-nuclear TOCSY and NOESY spectra and verified with 2D-experiments ^{13}C-HMQC and (HB)CB(CGCD)HD. NOE distance restraints were based on 3D-experiments, ^{13}C-edited NOESYHSQC and ^{15}N-edited NOESY HSQC, each acquired with a 150 ms mixing time. Semi-automated NOE cross-peaks were assigned using the CYANA software package (Güntert and Buchner, 2015) and were manually checked for correctness in an iterative manner. Dihedral angle restraints were predicted from the backbone chemical shifts using the program TALOS+ (Shen et al., 2009). Sixteen slowly exchanging backbone amide protons identified in the H/D exchange experiments were predicted to belong in α-helical regions by the chemical shift index analysis (Wishart and Sykes, 1994) and the NOESY patterns. Thus 32 corresponding distance restraints for HN-O and N-O atoms were imposed in the final structure calculation to depict the H-bonds (Williamson et al., 1985). Isotope-filtered NOESY experiments (3D-^{13}C,^{15}N-filtered/edited NOESY HSQC) were performed on a sample prepared by mixing a 1:1 ratio of unlabeled and ^{13}C,^{15}N-labeled sample to identify inter-subunit contacts between COA6 dimer. These experiments failed to reveal any cross peaks due to the weak dimerization constant and thus were not used in further analysis.

COA6 subunit structure calculation was performed using CYANA, version 3.96, following a torsion angle molecular dynamics protocol (Güntert et al., 1997). Two hundred random conformers were annealed in 15,000 steps for 7 cycles, and 20 structures with the lowest target functions after the final cycle were selected for water refinement, which was performed using the software X-plor NIH version, 2.50 (Schwieters et al., 2003). The structure ensemble was validated with the Protein Structure Validation Software suite 1.5 (Bhattacharya et al., 2007).

Relaxation Measurements

^{15}N relaxation experiments were performed on ^{15}N-labeled COA6 samples at 25°C on the 600 MHz spectrometer. Ten ^{15}N longitudinal relaxation rate constant (R1) experiments were performed in random order, with relaxation delays of 10 (duplicate), 90, 190, 320, 470 (duplicate), 660, 936, 1500 ms. Similarly, the transverse relaxation rate constant (R2) experiments were performed with relaxation delays of 0 (duplicate), 16.9, 33.9, 50.9 (duplicate), 67.8, 84.8, 118.7, 186.6 ms. Both rate constants were calculated using the program Curvefit, assuming a monoexponential decay of the peak intensities. The errors in the peak intensities were calculated from the two duplicate experiments. The steady-state heteronuclear [^{1}H]-^{15}N NOE experiment was carried out in an interleaved manner, with and without proton saturation and repeated thrice. The NOE effect was calculated as an average ratio of the peak intensities.

Online Liquid Chromatography-Inductively Coupled Plasma-Mass Spectrometry (LC-ICP-MS)

Cu binding to purified COA6 and COA6 within yeast mitochondrial extracts was measured using an online LC-ICP-MS system. A bioinert HPLC system (Agilent Technologies, 1260) located inside a chilled and refrigerated glove box (MBraun, labmaster 130) was connected to an ICP-MS (Agilent Technologies, 7700x) via PEEK tubing coming from the diode array of the LC system in the glove box. The HPLC system was composed of a pump (G5611A), diode array (G4212B), fraction collector (G5664A) and manual injector. The ICP-MS was interfaced with the LC system via a micromist nebulizer attached to a Scott-type spray chamber. The ICP-MS was tuned daily prior to analyzing samples. Samples were analyzed in helium collision mode. The instrument was tuned as described (Dziuba et al., 2018).

Samples were analyzed either with two Superdex Peptide 10/300 GL (GEHealthcare) columns connected in series or with a Bio SEC-3 (Agilent Technologies) column. Samples were passed through either a Titan regenerated cellulose 0.2 μm filter (Thermo scientific) or a 0.2 μm cellulose acetate filter (VWR). The dual peptide columns used a mobile phase of 20 mM Tris (pH 7.4) and 10 mM NaCl at a flow rate of 0.350 mL/min for a total of 160 min per run and a loop volume of 300 μL. The Bio SEC-3 column used a mobile phase of 20 mM Tris (pH 7.4) and 150 mM NaCl at a flow rate of 0.4 mL/min for a total of 10 min per run and a loop of 20 μL. The diode array was set for detection and data collection at 280 nm. Molecular mass standards were cyanocobalamin (1.3 kDa) from Fisher BioReagents and cytochrome *c* (12 kDa), carbonic anhydrase (30 kDa), albumin (66 kDa) and apoferritin (443 kDa) all from Sigma.

Gel-Filtration Chromatography

The apparent molecular mass of COA6 was determined using gel filtration chromatography. COA6 (100 μM) was loaded onto a Superdex 75 10/300 GL column equilibrated with 20 mM Tris (pH 7.4) and 150 mM NaCl at a flow rate of 0.3 ml/min. Aprotinin (6.5 kDa), cytochrome *c* (12.4 kDa), carbonic anhydrase (29 kDa) and albumin (66 kDa) were used as molecular weight references (Sigma, MWGF70).

Haddock Docking Calculation of the COA6:SCO1 Complex

The molecular docking of COA6 and SCO1 was performed using the Haddock d-level 2.2 web server as described (van Zundert and Bonvin, 2014). Chemical shift perturbation data were used as structural restraints (referred to as ambiguous interaction restraints (AIR)). The docking calculation used the NMR structure of COA6 determined in this study and the crystal structure of SCO1 (PDB: 2GVP) as input structures for the docking calculation. A total of 26 AIR restraints were used based on chemical shift perturbation data for COA6 (Figure 4A) and SCO1 (Figure 4C). Initial docking calculations generated 200 structures (with the lowest energy) that were then used for subsequent simulated annealing and water refinement. The final docked structures (10 lowest energy structures) had an overall RMSD of 1.8 Å.

SDS-PAGE and Western Blotting

Yeast mitochondrial proteins (20 μg) were separated by SDS-PAGE and blotted onto a polyvinylidene difluoride membrane. Membranes were treated for 1 hr in blocking buffer containing 5% nonfat milk dissolved in Tris-buffered saline with 0.1% Tween 20 (TBST-milk), followed by overnight incubation with primary antibody in TBST-milk at 4°C. Primary antibodies were used at the following dilutions: Cox2, 1:100,000 (Abcam 110271); Coa6, 1:5000 and Porin, 1:50,000 (Abcam 110326).

For the experiments with human cell lines, whole cells were homogenized on ice in STE buffer (250 mM sucrose, 10 mM Tris-HCl, pH 7.4, and 1 mM EDTA) supplemented with a 1 × cOmplete protease inhibitor cocktail (Roche, Indianapolis, IN) and 0.5 mM phenylmethylsulfonyl fluoride (PMSF; Sigma-Aldrich) and centrifuged twice at 4°C for 10 min at 600 × *g* to obtain a postnuclear supernatant. A crude mitochondrial fraction was then obtained by centrifugation at 4°C for 10 min at 8000 × *g* and used for non-reducing SDS–PAGE analyses as described (Leary and Sasarman, 2009). Alternatively, whole cells were extracted in a RIPA extraction buffer (50 mM Tris (pH 7.4), 150 mM NaCl, 1% Triton X-100, 0.5% sodium deoxycholate, 0.1% SDS, 1 mM EDTA and 1x Complete protease inhibitor cocktail), adjusted to a final concentration of 5 mg/ml, incubated on ice for 30 min and then centrifuged at 4 °C for 10 min at 14 000 × *g* and used for reducing SDS-PAGE analyses (Boulet et al., 2018).

For both reducing and nonreducing SDS–PAGE gels, equal amounts of protein were separated on precast gels (BioRad), transferred to nitrocellulose membrane, blocked for 2 hr in Tris buffered saline supplemented with 0.05% Tween 20 (TBST; 25 mM Tris (pH 7.4), 137 mM NaCl, 2.5 mM KCl and 0.05% Tween 20) containing 5% milk, and incubated overnight at 4 °C in primary antibody. Membranes were then washed six times for 5 min in TBST, incubated for 60 min in the appropriate horseradish peroxidase conjugated secondary antibody (BioRad, 1: 2500) in TBST containing 5% milk, and washed again in TBST as above. Primary

antibodies were used at the following dilutions: SCO1, 1:1000 (Bourens et al., 2014); SCO2, 1:1000 (Fitzgerald 70R-20118); COA6, 1:1000 (Proteintech 24209-1-AP); COX2, 1:1000 (Mitoscience MS405); GAPDH, 1:1000 (Cell signaling 14C10-2118) and Actin, 1:5000 (Bio-Rad 12004163). Membranes were developed using a homemade luminol-enhanced chemiluminescence solution, and visualized with the BioRad ChemiDoc MP Imaging System.

CcO Activity

Cco activity was measured as described (Capaldi et al., 1995). Briefly, we used triethanolamine/EDTA buffer to make a cell suspension, which is then added to a 96-well plate and the oxidation rate of cytochrome *c* was measured at 550nm. The activity assay was performed in potassium phosphate buffer (50mM pH 7) that contained cytochrome *c* and the mild detergent dodecylmaltoside.

Redox State Determination

The *in vitro* redox state of the cysteine residues in protein and protein mixtures were investigated by nonreducing SDS-PAGE after reaction of the samples with and without AMS as described previously (Morgada et al., 2015). Reduced and oxidized samples and protein mixtures (20–40 μM) were treated in an anaerobic environment with 1% (wt/vol) SDS and 10 mM AMS for 1 hr at 37°C, and resolved on 17% SDS-PAGE gels under nonreducing conditions.

Reduction Potential Determination

The midpoint reduction potential of the cysteine residues of COA6 was estimated by monitoring the redox state of thiols in COA6, using AMS and non-reducing SDS-PAGE after incubation in redox buffers. Samples of fully oxidized Coa6 (25 mM) were incubated for 24 hr in 50 mM phosphate pH 7 buffer with different ratios of oxidized and reduced DTT. Reduced DTT and Oxidized DTT solutions were prepared by dissolving the solid form of each (sigma Aldrich D0632 and D3511 respectively) in 50 mM nitrogen-fluxed potassium phosphate buffer (pH 7) under anaerobic conditions. The redox potential of the buffers (E_{Buff}) was estimated using the Nernst equation: $E_{Buff} = E_0 + 29.4\log([DTTox]/[DTT]^2)$ with E_0 being −332 mV for the DTT redox couple at pH 7.0 using with a 1 mM being the maximal concentration of reduced DTT. After incubation, reactions were quenched by addition of 5 mM AMS (Thermo Fisher A485), 2% SDS and incubated at 37°C for 1 hr. Non-reducing protein loading buffer was added to the samples and the redox state of the proteins was followed by SDS-Gel shift assay in 16% polyacrylamide gel. The reduced fractions were quantified using the ImageJ software.

In Vitro Labeling of Mitochondrial Translation Products

Cells were labeled in 6 cm dishes as described in detail elsewhere (Leary and Sasarman, 2009). Briefly, cells were incubated in chloramphenicol (Sigma) prior to labeling to inhibit mitochondrial translation and allow for the accumulation of nuclear-encoded respiratory chain subunits. 400 μCi of a [^{35}S]-methionine and cysteine mixture (Easy Tag EXPRESS) was added for 60 min to cells in methionine- and cysteine-free DMEM containing 10% dialyzed fetal bovine serum (GIBCO) and anisomycin (Sigma), to reversibly inhibit cytoplasmic translation. Total cellular protein (50 μg) was resuspended in sample loading buffer containing β-mercaptoethanol, sonicated and run on a 12%–20% gradient gel. Gels were subsequently transferred to nitrocellulose under semi-dry conditions and the [^{35}S]-labeled mitochondrial translation products were detected through digital autoradiography.

QUANTIFICATION AND STATISTICAL ANALYSIS

Data are shown as mean ± standard deviation (SD) or mean ± standard error of the mean (SEM), and the number of replicates is indicated in the figure legends. Values of $p < 0.05$ were considered significant. Statistical analysis was performed using GraphPad Prism version 8 (GraphPad Software, La Jolla California USA, https://www.graphpad.com).

DATA AND CODE AVAILABILITY

The solution structure of human COA6 isoform 3 has been deposited in the Protein Data Bank with the accession code PDB: 6NL3.

Cell Reports, Volume *29*

Supplemental Information

COA6 Is Structurally Tuned to Function as a Thiol-Disulfide Oxidoreductase in Copper Delivery to Mitochondrial Cytochrome *c* Oxidase

Shivatheja Soma, Marcos N. Morgada, Mandar T. Naik, Aren Boulet, Anna A. Roesler, Nathaniel Dziuba, Alok Ghosh, Qinhong Yu, Paul A. Lindahl, James B. Ames, Scot C. Leary, Alejandro J. Vila, and Vishal M. Gohil

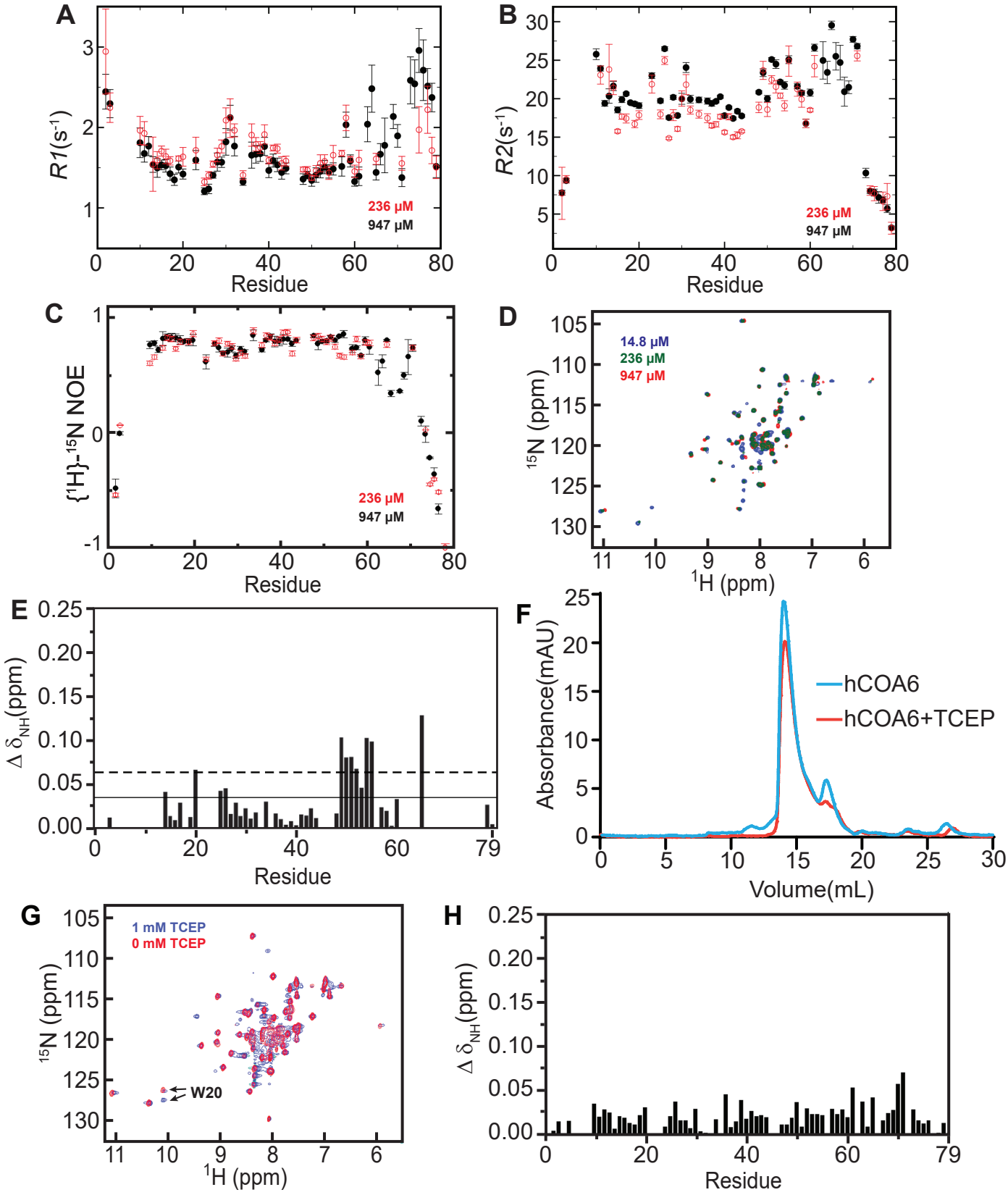

Figure S1 (related to Figure 1). Interrogation of COA6 structure by NMR.
(A) Longitudinal relaxation rates (R1), (B) transverse relaxation rates (R2), and (C) Heteronuclear ^{1}H-^{15}N NOEs, are plotted as a function of residue number for COA6 at two different protein concentrations. (D) Overlay of the ^{1}H-^{15}N HSQC spectra of human COA6 at three different protein concentrations: 14.8 μM (blue), 236 μM (green) and 947 μM (red). (E) Average chemical shift deviation of ^{15}N-labeled COA6 at 947 μM TCEP when compared to treatment with 14.8 μM TCEP. The horizontal solid line represents the mean and the dashed line represents the mean + SD of chemical shift perturbation for all residues. (F) Elution profile of COA6 from a Superdex 75 gel filtration column in the presence and absence of 1mM TCEP. (G) Overlay of the ^{1}H-^{15}N HSQC spectra of human COA6 with and without 1mM TCEP. (H) Average chemical shift deviation of ^{15}N-labeled COA6 upon addition of 1mM TCEP.

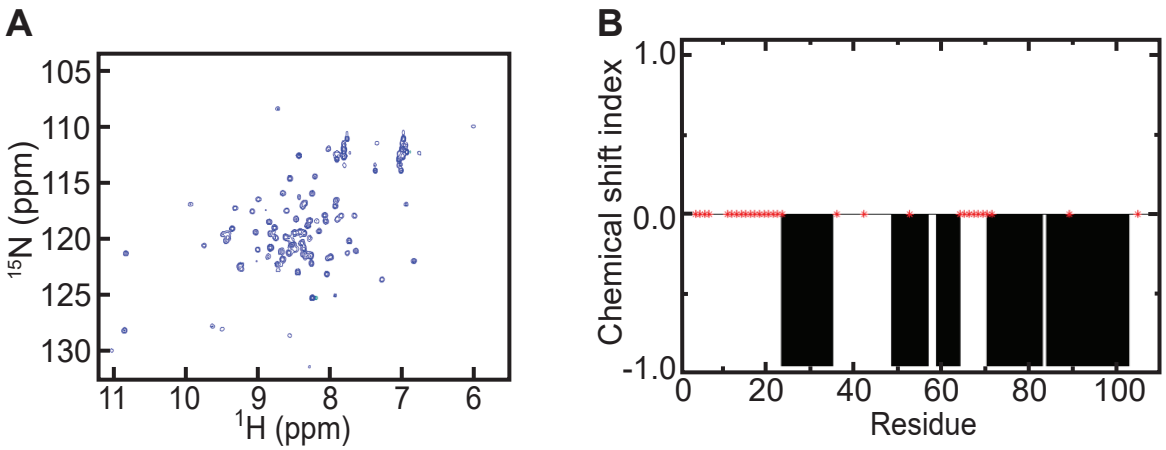

Figure S2 (related to Figure 1). Yeast Coa6 is a helical protein.
(A) ^{1}H-^{15}N HSQC spectrum of yeast Coa6. (B) The chemical shift index is shown as a function of residue number. Negative values represent an α-helical propensity, while positive values are indicative of a β-strand. A red asterisk denotes residues which were unassigned.

A

```
SCO1 SFTGKPLLGGPFSLTTHTGERKTDKDYLGQWLLIYFGFTHCPDVCPEELEKMIQVVDEID 189
SCO2 ---GSFTGQGDFHLLDHRGRARCKADFRGQWVLMYFGFTHCPDICPDELEKLVQVVRQLE 152
        *.    * * *  * *. : . *: ***:*:**********:**:****::*** :::
SCO1 SITTLPDLTPLFISIDPERDTKEAIANYVKEFSPKLVGLTGTREEVDQVARAYRVYYSPG 349
SCO2 AEPGLPPVQPVFITVDPERDDVEAMARYVQDFHPRLLGLTGSTKQVAQASHSYRVYYNAG 212
     :    ** :*:**::*****  **:*.**::* *:*:****: ::* *.:::*****. *
SCO1 PKDEDEDYIVDHTIIMYLIGPDGEFLDYFGQNKRKGEIAASIATHMRPYRKKS- 301
SCO2 PKDEDQDYIVDHSIAIYLLNPDGLFTDYYGRSRSAEQISDSVRRHMAAFRSVLS 266
     *****:******:* :**:.*** * **:*:.:   :*: *:  **  :*.
```

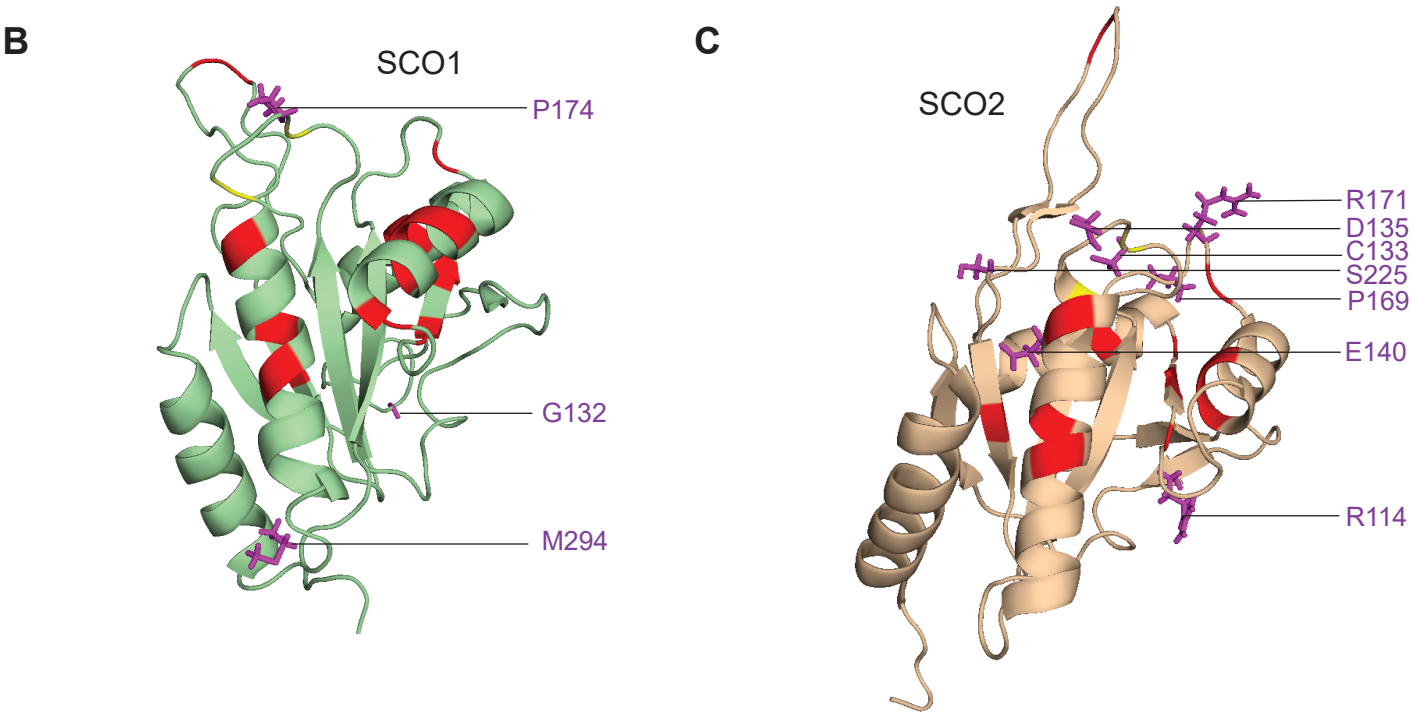

Figure S3 (related to Figure 4). A subset of human patient mutations in SCO1 and SCO2 are in close vicinity to the COA6 interaction surface.

A) Alignment of human SCO1 and SCO2 proteins. The amino acids shown in red undergo chemical shift perturbation in the presence of COA6, which is indicative of their involvement in an interaction. The residues shown in red and bold are the residues that are identical or similar in both SCO proteins. B) SCO1 (PDB: 2GVP) and SCO2 (PDB:2RLI) amino acid residues that interact with COA6 are highlighted in red and side-chains of the residues mutated in human patients are depicted in purple. Patient mutations listed here are from OMIM database (OMIM:603644, OMIM:604272) and from Leary et al., 2013 and Rebelo et al., 2018.

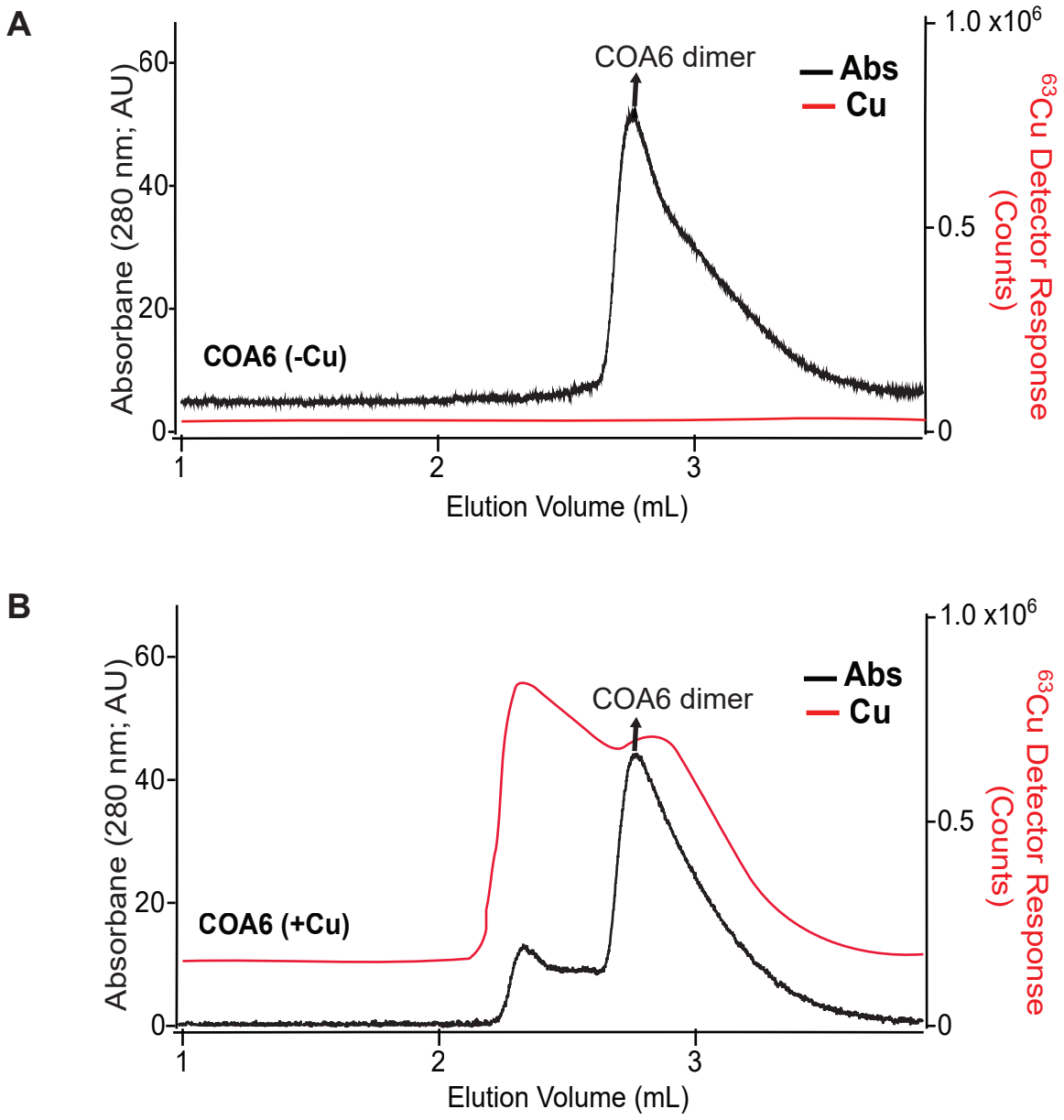

Figure S4 (related to Figure 5). Recombinant COA6 only binds copper when reconstituted with the metal ion and reductant.

(A) ^{63}Cu and protein traces of recombinant COA6 analyzed by LC-ICP-MS. (B) ^{63}Cu and protein traces of recombinant COA6 reconstituted with $CuSO_4$ and reduced glutathione.

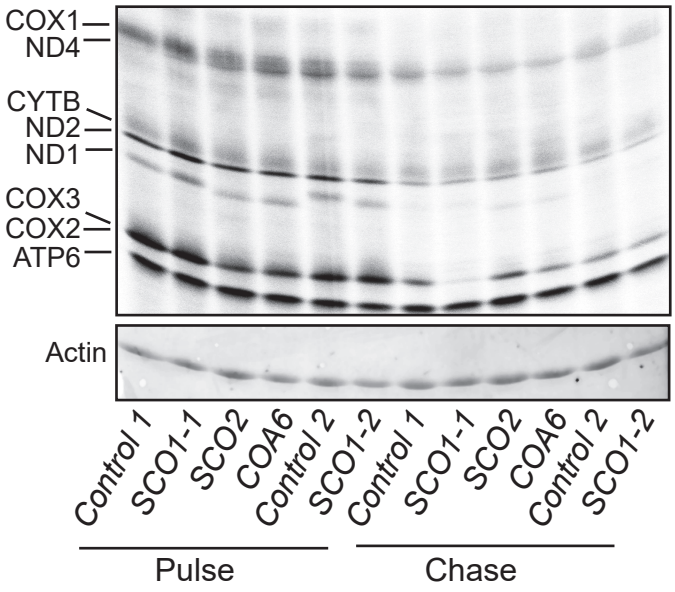

Figure S5 (related to Figure 6). Impact of SCO1, SCO2 and COA6 mutations on the synthesis and turnover of COX2.

In vivo ^{35}S-labeling of mitochondrial translation products in control and patient cell lines. Samples were pulse-chased and analyzed by SDS-PAGE and digital autoradiography.

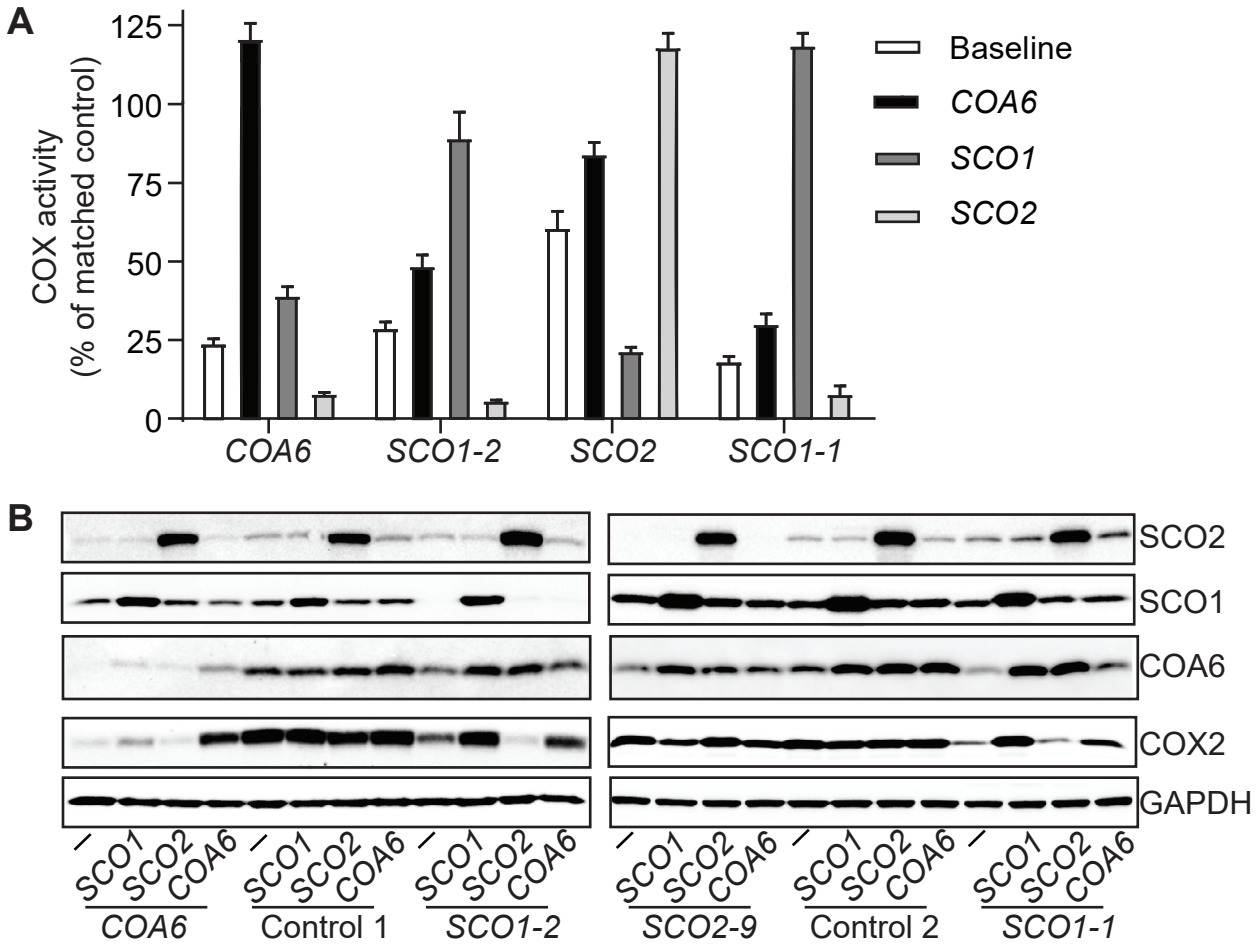

Figure S6 (related to Figure 6). Epistasis analysis of SCO1, SCO2 and COA6 overexpression on CcO activity in patient cell lines.

(A) Cytochrome c oxidase acitvity (CcO) in *COA6, SCO1* and *SCO2* patient cell lines alone (baseline) or when overexpressing COA6, SCO1 or SCO2. Data are represented as mean + SEM. (B) SDS-PAGE/Western blot analysis of COA6, SCO1, SCO2, COX2 and GAPDH (loading control) abundance in protein lysates from control and patient cells described in Figure A.

Table S1 (related to Figure 1). NMR and refinement statistics for solution structure of COA6

NMR distance and dihedral constraints	
Distance restraints	
Total NOE	554
Intra-residue	163
Inter-residue	284
Sequential ($\|i - j\| = 1$)	177
Nonsequential ($\|i - j\| > 1$)	214
Long-Range NOE	107
Hydrogen bonds	32
Total dihedral angle restraints	108
ϕ (TALOS+)	54
ψ (TALOS+)	54
Structure statistics	
Violations (mean and s.d.)	
Distance constraints (Å)	0.01 ± 0.03
Dihedral angle constraints (º)	0.37 ± 0.88
Max. dihedral angle violation (º)	6.18
Max. distance constraint violation (Å)	0.43
Deviations from idealized geometry	
Bond lengths (Å)	0.008
Bond angles (º)	0.6
Ramachandran Plot	
Most favored	79.6%
Additionally allowed	17.2%
Generously allowed	3.2%
Disallowed	0.1%
Average pairwise r.m.s. deviation* (Å)	
Protein structured region (residues 9 to 64)	
Heavy	1.35
Backbone	0.54

*Pairwise r.m.s. deviation was calculated among 20 refined structures.

Table S2. Related to STAR Methods. Primers used in this study.

Name	Sequence (5' to 3')
Protein expression primers	
Human COA6 isoform 3 Forward	GGGCCAGGATCCATGGCAGCACCGAGCATGAAA
Human COA6 isoform 3 Reverse	GGGCCACTCGAGTTAGCTTTTTGCGGTGGTTTC
Yeast Coa6 Forward	TAGCGAAAATCTGTATTTTCAGGGTAGCGAATTCATGGGC TTATTTTCATTTGATGGTGGC
Yeast Coa6_Stop Reverse	GTGGTGGTGGTGGTGCTCGAGTCACTGATTTCGTTCCCT CTGTTTAG
Yeast Coa6 Reverse	GTGGTGGTGGTGGTGCTCGAGCTGATTTCGTTCCCTCTG TTTAG
Site Directed mutagenesis primers	
HyCOA6 W26C Forward	AGTATTCATCTCTAGCACCGCAACACAATTTTCTTTGGG
HyCOA6 W26C Reverse	CCCAAAGAAAATTGTGTTGCGGTGCTAGAGATGAATACT
HyCOA6 W33R Forward	TTTTCGTCCAAACATTTCCGGTATTCATCTCTAGCACCC
HyCOA6 W33R Reverse	GGGTGCTAGAGATGAATACCGGAAATGTTTGGACGAAAA
HyCOA6 E54X Forward	CATTGTTGTGGACAAGAAGATTAGAAAGAGGATCTCAACT TCTTA
HyCOA6 E54X Reverse	TAAGAAGTTGAGATCCTCTTTCTAATCTTCTTGTCCACAAC AATG
Primers for Human COA6	
COA6-F	AAAAAGCAGGCTACCATGGGCCCGGGAGGTCCCTT
COA6-R	AGAAAGCTGGGTCTAGGATTTTGCAGTTGTTTCTGA
COA6 W59C-F	GAAAGACAGGTCTGCTGTGGGGCCCGGGATGAGTAC
COA6 W59C-R	GTACTCATCCCGGGCCCCACAGCAGACCTGTCTTTC
COA6 W66R-F	GCCCGGGATGAGTACCGGAAGTGTTTAGATG
COA6 W66R-R	CATCTAAACACTTCCGGTACTCATCCCGGGC
Protein truncation primers	
HyCOA6 SacI Forward	CCCCTGGAGCTCGCAAAGACGCGCAGCCAAAAA
HyCOA6_64 BamH1 Reverse	GCGCGCGGATCCCTTTTCTTTGAACTTCAAGTAGTCTCT
HyCOA6_72 BamH1 Reverse	GCGCGCGGATCCTGGTTCGAATTGACCGGCTTCGAACTT